Biomedicine & Pharmacotherapy 170 (2024) 116056

Contents lists available at ScienceDirect

Biomedicine & Pharmacotherapy

journal homepage: www.elsevier.com/locate/biopha

Evaluation of pro-regenerative and anti-inflammatory effects of isolecanoric acid in the muscle: Potential treatment of Duchenne Muscular Dystrophy

Lidia Matias-Valiente [a,b], Cristina Sanchez-Fernandez [a,b], Lara Rodriguez-Outeiriño [a,b], Maria C. Ramos [b], Caridad Díaz [b], Gloria Crespo [b], Victor González-Menéndez [b], Olga Genilloud [b], Fernando Reyes [b], Marisol Montolio [d,e], Francisco Hernandez-Torres [b,c,*], Amelia Eva Aranega [a,b,**]

[a] Cardiovascular Development Group, Department of Experimental Biology, Faculty of Experimental Sciences, University of Jaen, Jaen, Spain
[b] Fundación MEDINA, Technology Park of Health Sciences, Granada, Spain
[c] Department of Biochemistry and Molecular Biology III and Immunology, Faculty of Medicine, University of Granada, Granada, Spain
[d] Department of Cell Biology, Physiology and Immunology, Faculty of Biology, University of Barcelona, Spain
[e] Duchenne Parent Project Spain Madrid, Spain

ARTICLE INFO

Keywords:
Duchenne muscular dystrophy
Muscle stem cells
Inflammatory response
Natural products
Isolecanoric acid

ABSTRACT

Duchenne muscular dystrophy (DMD) is a devastating degenerative disease of skeletal muscles caused by loss of dystrophin, a key protein that maintains muscle integrity, which leads to progressive muscle degeneration aggravated by chronic inflammation, muscle stem cells' (MuSCs) reduced regenerative capacity and replacement of muscle with fibroadipose tissue. Previous research has shown that pharmacological GSK-3β inhibition favors myogenic differentiation and plays an important role in modulating inflammatory processes. Isolecanoric acid (ILA) is a natural product isolated from a fungal culture displaying GSK-3β inhibitory properties. The present study aimed to investigate the proregenerative and anti-inflammatory properties of this natural compound in the DMD context. Our results showed that ILA markedly promotes myogenic differentiation of myoblasts by increasing β-Catenin signaling and boosting the myogenic potential of mouse and human stem cells. One important finding was that the GSK-3β/β-Catenin pathway is altered in dystrophic mice muscle and ILA enhances the myofiber formation of dystrophic MuSCs. Treatment with this natural compound improves muscle regeneration of dystrophic mice by, in turn, improving functional performance. Moreover, ILA ameliorates the inflammatory response in both muscle explants and the macrophages isolated from dystrophic mice to, thus, mitigate fibrosis after muscle damage. Overall, we show that ILA modulates both inflammation and muscle regeneration to, thus, contribute to improve the dystrophic phenotype.

1. Introduction

Duchenne muscular dystrophy (DMD) is a severe progressive disease that affects approximately 1 in 5000 live male births [1–4]. DMD is characterized as a muscular disorder caused by mutations in the dystrophin gene located on the short arm of the X chromosome. The absence of, or defects in, dystrophin levels results in chronic inflammation, progressive muscle degeneration and replacement of muscle with fibroadipose tissues [5,6]. Although today many individuals with DMD are now living to their 30 s and beyond, these patients' premature death is irretrievable and usually results from cardiac or respiratory compromise [7–10]. There is currently no cure for DMD [11,12]. Lack of efficacious established treatment makes the evaluation of different approaches necessary in an attempt to treat affected patients [13]. In DMD, progressive muscle wasting and weakness are associated with the exhaustion of muscle regeneration, which is potentially linked with

* Correspondence to: Dept. of Biochemistry, Molecular Biology III, and Immunology, School of Medicine. University of Granada, Avda. de la Investigación, 11. PC 18016, Granada, Spain.
** Correspondence to: Dept. of Experimental Biology, Faculty of Experimental Sciences. University of Jaen, Paraje las Lagunillas s/n. PC 2307, Jaen, Spain.
E-mail addresses: fhtorres@ugr.es (F. Hernandez-Torres), aaranega@ujaen.es (A.E. Aranega).

https://doi.org/10.1016/j.biopha.2023.116056
Received 15 November 2023; Received in revised form 19 December 2023; Accepted 21 December 2023
Available online 29 December 2023

intrinsic defects in muscle stem cell functions [11,14]. Skeletal muscle has the ability to repair and regenerate due to the presence of resident stem cells, termed muscle satellite cells or MuSCs [15]. There are cumulative pieces of evidence for MuSCs involvement in muscular dystrophies in which these cells apparently fail to efficiently repair muscle damage. We and others have previously demonstrated that dystrophic MuSCs exhibit severe defects in cell proliferation, together with lower myogenic potential [15–19]. Hence the development of new approaches to modify the regenerative capability of dystrophic satellite cells becomes very important for creating new therapies for DMD. In relation to lack of regenerative capacity, chronic inflammation contributes substantially to muscle damage and age-related muscle replacement with fibrofatty tissue. Indeed chronic inflammation with the persistent production of profibrotic cytokines leads to endomysial fibrosis, which directly contributes to progressive muscle dysfunction and the lethal DMD phenotype [20]. Currently, the DMD care standard is corticosteroids, which aim to delay disease progression by reducing inflammation-induced muscle damage and, thus, muscle strength loss and disease progression [21,22]. However, their prolonged administration generates a series of side effects that strongly affect patients' life quality [23,24]. In this scenario, it is imperative to find alternative drugs that modulate the inflammatory response while minimizing these side effects.

Glycogen synthase kinase-3β (GSK-3β), a dual-specificity kinase involved in many signaling and metabolic pathways [25], plays a central role in the regulation of the Wnt/β-Catenin signaling pathway. Wnt signals promote β-catenin nuclear translocation through GSK-3β inhibition to, this, allow thus β-Catenin-mediated activation of their target genes [26]. It has been previously demonstrated that β-CATENIN targets myogenic determinants genes (*Myf5 and Myod1*) in muscle precursor cells by facilitating myogenic differentiation during both embryonic and adult myogenesis [27–29]. Previous reports have shown that GSK-3β inactivation mediated by Wnt signaling is a critical determinant of cell fate in MuSC progeny and myoblasts differentiation. In line with this, it has been reported how the stabilization of β-CATENIN mediated by the GSK-3β inhibition increases progression toward myogenic lineage and, thus, facilitates muscle regeneration in mice [29]. It has also been shown that pharmacological GSK-3β inhibition considerably improves the in vitro differentiation of myogenic precursor cells (myoblasts) [30]. All these data lead us to hypothesize whether pharmacological GSK-3β inhibition could positively impact DMD progression by improving the myogenic differentiation of dystrophic MuSCs. In parallel, the importance of GSK-3β in regulating the levels of pro-and anti-inflammatory cytokines in innate immune cells has been previously reported. Thus pharmacological GSK-3β inhibition with a panel of different GSK-3β-selective inhibitors suppresses the production of pro-inflammatory molecules IL-1β, IL-6, TNF, and IL-12, whereas the production of anti-inflammatory IL-10 increases in stimulated monocytes [31]. Moreover, the importance of GSK-3β in controlling the inflammatory response has been confirmed in mouse embryonic fibroblasts that were deficient in this enzyme [32]. Altogether, these results suggest that GSK-3β inhibition might be a point of convergence to modulate both regeneration and inflammatory response in muscle.

Isolecanoric acid (ILA), a natural product isolated from strain CF-160870 of the fungus *Glarea lozoyensis,* has been previously described as a GSK-3β inhibitor and protector in neurodegenerative in vitro models by de Pedro *et al.* 2016 [33]. These properties, together with its low cytotoxicity, make it an interesting candidate to test in the DMD model. Hence, the current study evaluated the proregenerative and chronic anti-inflammatory potential of ILA in myoblasts and dystrophic muscle by using in vitro and in vivo methods. Moreover, in vivo acute toxicity and ILA pharmacokinetics were also investigated.

2. Material and methods

2.1. ILA production

Twelve mycelial discs of the fungus *Glarea lozoyensis* CF-160870, ATCC-20868 (Ascomycota, Leotiomycetes) were used to inoculate 50 mL of SMYA medium (10 g Difco neopeptone, 40 g maltose, 10 g Difco yeast extract, 3.5 g agar, 1 L distilled H_2O). After 7 incubation days at 22 ^oC, 220 rpm and 70% relative humidity (RH), 4.5 mL aliquots of this culture were used to inoculate MSPM medium (75 g maltose, 1 g soybean I (Sigma-Aldrich), 3 g L-proline, 4,3 g Murashine & Skoog Salts; 1 L distilled H_2O), distributed in 120 Erlenmeyer flasks (500 mL), each containing 100 mL of culture medium. Flasks were incubated at 22 ^oC, 220 rpm and 70% RH for 14 days.

The 12 L culture was extracted by the addition of an equal volume of acetone, with shaking for 3 h, centrifugation at 9500 rpm for 15 min and filtration in a vacuum. The remaining liquid was evaporated under a nitrogen stream to a final volume of 9 L and loaded into three SP207ss columns (3 × 65 g). Columns were eluted with a water/acetone stepped gradient (10 mL/min; 10–100% acetone in 40 min; 100% acetone for 15 min, 20 mL per fraction). Fractions were analyzed by LC/MS. Those containing the compound of interest were pooled and subjected to a second flash chromatography in reversed phase RP18 (4 columns of 3.5 × 12 cm). Each column was eluted with a water/acetonitrile gradient from 10% to 100% acetonitrile in 55 min with a final wash step of 10 min at 100% acetonitrile (18 mL/min, 18 mL per fraction). The fractions from this chromatographies containing ILA as determined by LC/MS were further purified by reversed phase HPLC using an Agilent Zorbax SB-C8 Prep^{HT} column (21.2 × 250 mm), a gradient water/acetonitrile (5%−50% acetonitrile in 35 min, 20 mL/min, UV detection at 210 and 266 nm) to yield 579 mg of a white amorphous solid (rt: 19.5 min), which was identified as ILA (Fig. 1**A**) by making comparison of its spectroscopic data to those reported elsewhere [34].

2.2. Sol8 cells culture

Sol8 myoblasts (ATCC, CRL-2174) were seeded at 250,000 cells/well in a 6-well plate in Sol8 growth medium (DMEM, 20% FBS and 1% P/S) and incubated at 37ºC, 5% CO_2. After 24 h, when cells adhered to the culture dish surface, the medium was replaced with differentiation medium (DMEM, 2% FBS, 1% P/S) and treated with 25 μM or 50 μM ILA. As a negative control, only DMSO was added to Sol8 myoblasts. Sol8 myoblasts were collected at 24 h after treatment by a Western Blot assay and 72 h for the RT-qPCR and immunocytochemistry assays.

2.3. Mouse and human MuSCs isolation and culture

For the mouse MuSCs, isolation was performed by Magnetic cell isolation (MACS) as described by Rodriguez-Outeiriño et al. (2022) [19]. Briefly, hind limb muscles from 4-month-old male mice (wild-type C57BL/10ScSn (IMSR_JAX:000476) and dystrophic C57BL/10ScSn-Dmd^{mdx}/J (IMSR_JAX:001801)) were collected, transferred to and minced on a dish with DMEM-F12 and dissociated for 1 h at 37ºC in an enzymatic solution containing DMEM: F12 supplemented with 1 mg/mL collagenase type D and 4% Trypsin solution. Afterward, mechanical dissociation was performed through 14 G and 18 G needles and filtered through 100 μm and 40 μm cell strainers. The flowthrough material was incubated for 2 min in Red Blood Cells Lysis Solution (Miltenyi Biotec, 130–094-183). Subsequently, the incubation with magnetic labeling was performed for 15 min at 4ºC of 1:5 dilution according to the MicroBeads Satellite Cell Isolation Kit: negative selection with the Satellite Cell Isolation Kit (Miltenyi Biotec, 130–104-268) and positive selection with Anti-Integrin a-7 MicroBeads (Miltenyi Biotec, 130–104-261). Purified mouse MuSCs (5000–10000 cells) were seeded on a 6-well plate and cultured in mouse growth medium containing DMEM-F12 supplemented with 20% FBS, 2% Ultroser G (Pall,

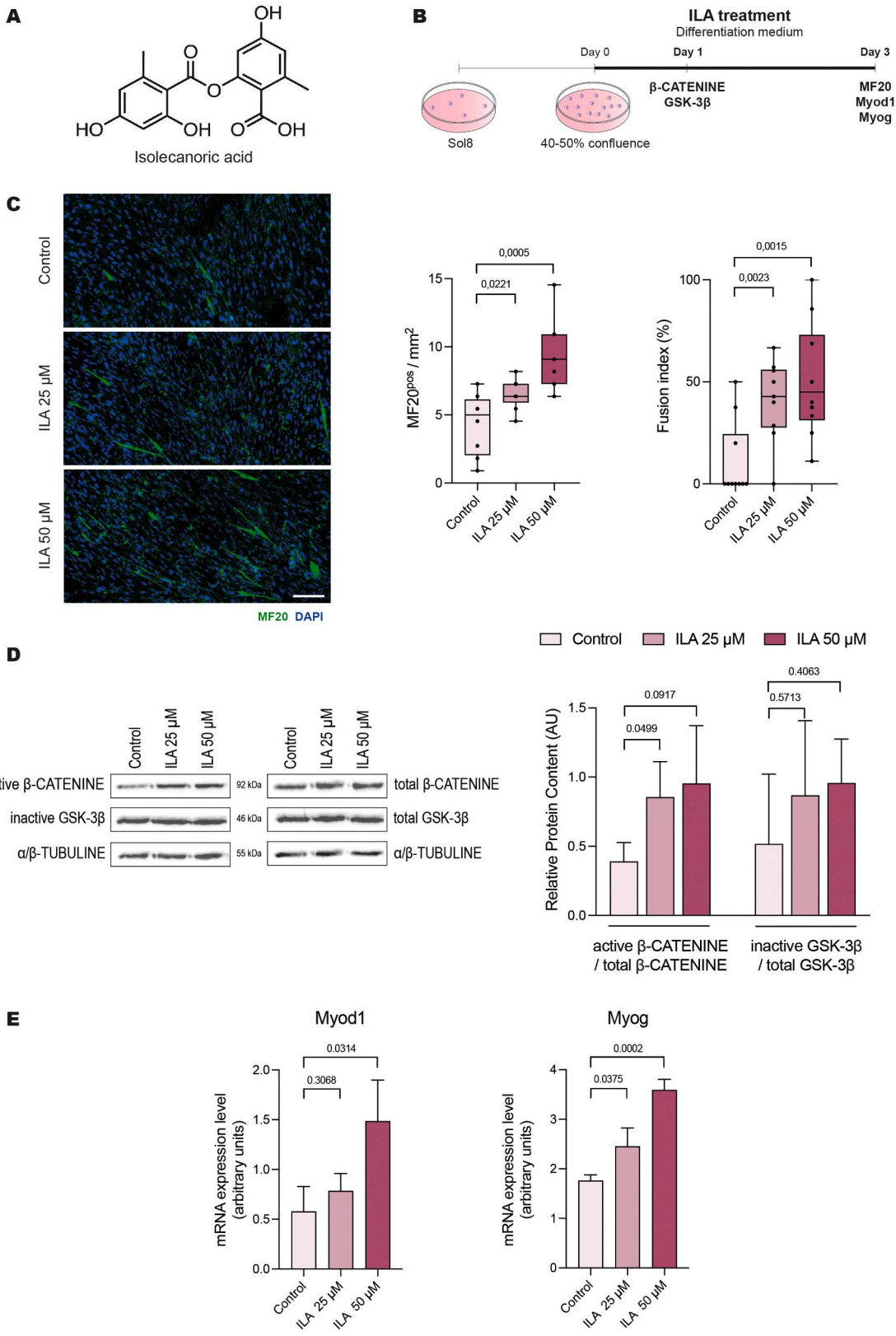

Fig. 1. ILA compound increments myoblast differentiation by increasing β -CATENINE through GSK-3β inhibition. (A) Scheme of the chemical structure of isolecanoric acid (ILA). (B) Scheme of ILA treatment in the Sol8 myoblasts cultured under differentiation conditions (n = 3 per condition). (C) Representative images of MF20 staining in the Sol8 myoblasts treated at different ILA doses, the quantification of the number of $MF20^{pos}$ cells per area and the Fusion Index after 3 days of ILA treatment (n = 3 independent experiment, 5 aleatory fields per condition). Scale bar: 100 µm. (D) Western blot and quantification for the relative protein content of the active β-CATENINE versus the total β-CATENINE, as well as the inactive GSK-3β versus the total GSK-3β in Sol8 myoblast after 24 h of ILA treatment. α/β-TUBULINE was used as the normalization protein (n = 3 independent experiment per condition). (E) RT-qPCR for Myod1 and Myogenin (Myog) after 3 days of ILA treatment (n = 3 independent experiment per condition).

15950–017), 3% penicillin/streptomycin (onward P/S; Sigma-Aldrich, P0781), and incubated at 37ºC, 5% CO_2. For myoblast differentiation, when 70% to 80% confluence was reached, the medium was changed by decreasing to 2% FBS. ILA treatment was added at 25 μM and 50 μM dissolved in DMSO. These were the concentrations tested from that point onward in accordance with the concentrations previously tested by de Pedro et al. (2016) [33]. As the negative control, only DMSO was added to human myoblasts. Mouse myoblasts were collected for the immunocytochemistry assays.

Human SCs (hMuSCs) were obtained from fresh Sartorius muscle biopsies from a 40-year-old male during varicose veins surgery. This patient had no other acute or chronically illness. hMuSCs isolation was performed by MACS as previously described for mice. Briefly, muscle fascicles were released and cut into 3-μm fragments in the HBSS supplemented with 1% PSF (P/S-Fungizone (Gibco Life Technologies, 15290–018)). Fascicles were incubated overnight at 37ºC, 5% CO_2, in conditioning medium containing M199 supplemented with 37.5% FBS and 1% PSF. The next day, explants were seeded on the plates coated with 25% v/v fresh human plasma until cell growth appeared. Subsequently, explants were cut into 1-mm-length fragments and cultured on 33.3% v/v fresh human plasma-1.5% gelatin type-A coated plates until the cell monolayer appeared around explants. Positive cell sorting was performed using CD56-human MicroBeads (130- 050–401; Miltenyi). $CD56^{pos}$ hMuSCs cells were seeded at 55,000 cells/well on 0.1% gelatin type-A coated 6-wells plates and cultured in human growth medium containing 75% DMEM High Glucose pyruvate, and 25% M199 supplemented with 10% FBS, 50 mg/mL insulin (Sigma-Aldrich, I5500), 0.25 mg/mL human-FGF2 (Peprotech, 100–18B), 0.02 mg/mL human-EGF (Peprotech, AF-100–15), 2 mM L-glutamine (Sigma-Aldrich, G7513) and 1% PSF. When 70% to 80% confluence was reached, hMuSCs were incubated at 37ºC, 5% CO_2, with differentiation medium (with FBS lowering to 2%) in the absence or presence of ILA (25 μM or 50 μM). As a negative control, only DMSO was added to human myoblasts. The final hMuSCs differentiation was viewed and analyzed by optical inverted microscope (Motic, AE2000).

2.4. Muscle explants culture

The hind limb muscles from 4-month-old mice were finely diced and placed in DMEM at 37 °C in a humidified atmosphere of 21% O_2 and 5% CO_2 for 1 h. Muscle tissue was centrifuged for 5 min at 200g, and approximately 50 mg were transferred to 24-well tissue culture plates with 1 mL DMEM and 1% P/S. Muscle explants were incubated in the absence or presence of 25 or 50 μM ILA for 60 min before the addition of 10 μg/mL LPS (Sigma-Aldrich, L2880) for 20 h. After the final incubation, tissue and media were collected separately and stored at − 80 °C for further analyses, as detailed below.

2.5. Macrophages isolation and culture

Bone marrow-derived macrophages (BMDMs) isolation was performed as described by Ying, W. et al. (2013) and Toda et al. (2021) [35,36]. Briefly, the femur and tibia from 4-month-old mdx mice were extracted and cleaned in cold 1 × PBS. Then bone marrow was flushed out into cold 1 × PBS + 2% FBS using a 21 G needle and a 10 mL syringe, and passed through the needle 4–6 times to dissociate cells. The cell suspension was centrifuged at 200g for 5 min, filtered through a 70-μm cell strainer, and incubated with 500 μL 1 × PBS and 5 mL 1 × Blood Cell Lysis Solution (Miltenyi Biotec, 130–094-183). After further centrifugation at 500g for 5 min at 4ºC, cells were incubated with BMDMs specific growth medium: IMDM supplemented with + 10% FBS + 10 nm/mL M-CSF (Peprotech, 315–03). On day 3, the BMDMs growth medium was refreshed. On day 7, the mature BMDMs were detached using ice-cold 5 mM PBS-EDTA and incubated for 40 min at 4ºC with Brilliant Stain Buffer (BD Horizon™, 563794), together with fluorophore-conjugated antibodies (listed in Table 1) to detect the cells expressing specific macrophage markers using the BD FACSymphony™ A5 Cell Analyzer.

Table 1
Antibodies used in flow cytometry.

Primary Antibody	Source	Concentration	Company	Identifier
BB515 Anti-CD11b	Rat	5 μg/mL	BD Horizon™	564454
Anti-Mouse F4/80	Rat	5 μg/mL	BD Horizon™	565787
BV421 Anti-Mouse CD11c	Hamster	5 μg/mL	BD Horizon™	562782
PE Anti-Mouse CD206	Rat	5 μg/mL	BD Horizon™	568273

BMDMs (approx. 250000 cells/well in a 6-well plate) were incubated for 24 h in the absence or presence of 25 or 50 μM ILA, together with 100 ng/mL LPS. BMDMs were detached and used for the RT-qPCR analysis.

2.6. In vitro toxicity assays

2.6.1. Drug-drug interaction

Drug-drug interaction was performed using human liver microsomes and evaluating the production of specific substrates for the main CYP450 isoforms by liquid chromatography-mass spectrometry analysis. ILA was tested for its inhibitory activity of CYP3A4, CYP2D6 and CYP2C9 isoforms by using a previously described methodology [37].

2.6.2. In vitro cardiotoxicity

Cardiotoxicity was determined by measuring the activity on the potassium ion channel human ether-à-go-go-related gene (hERG), L-type calcium channel Cav1.2 and voltage-gated Na+ channel Nav1.5. For the study of the hERG channel, HEK 293-hERG cells stably express functionally active hERG potassium channels (B'SYS) were used in the FluxOR™ potassium channel assay (Invitrogen) according to the manufacturer's instructions [38]. The Cav1.2 channel was investigated using a functional assay based on a fluorescent probe (Fluo-4AM, Invitrogen). Hek_293 cells express Cav1.2 calcium channel (Fundacion MEDINA) were incubated in poly-D-lysine-treated black 384-well plates for 24 h. After the incubation with the probe for 30 min, cells were incubated with compounds for 30 min in the same buffer, followed by the addition of a high concentration of potassium (85.5 mM K+) [38]. The Nav1.5 channel was assayed using a functional assay based on the changes in membrane potential brought about by compounds that modulate or block voltage-gated Na+ channels using FLIPR Membrane Potential Assay dye (Molecular Devices), following the manufacturer's instructions [39] and, the cell line Hek_293 cells express Nav1.5 sodium channel (Fundacion MEDINA). These assays were performed on a FLIPR Tetra® High Throughput Cellular Screening System (Molecular Devices).

2.6.3. AMES test

A commercial test kit, AMES MPFTM 98/100 Microplate Format Mutagenicity Assay, from Xenometrix AG 4228 (Allschwil, Switzerland), was used to evaluate the mutagenicity of isolecanoric acid with and without metabolic activation S9 using amino acid requiring S. typhimurium strains TA100 and TA98.

2.7. In vivo toxicity assay

ILA was prepared in 10% DMSO and 40% cyclodextrin (Sigma-Aldrich, 332607) at 150, 105, 75 and 30 mg/mL. Some precipitates were detected at 150 mg/mL. Therefore, maximum solubility was set at 105 mg/mL. Then preparations of 105, 75 and 30 mg/mL of the compound, which corresponded to 250, 150 and 100 mg/kg, and the vehicle (100 μL), were administered intraperitoneally (IP) to the 4-month-old

wild-type mice (N = 12 mice, n = 3 per condition). A daily supervision protocol was applied.

2.8. Pharmacokinetic study

The 4-month-old wild-type mice were treated IP at the single dose of lower ILA dose testes in the toxicity assay (100 mg/kg). Twenty-seven mice were randomized in nine groups for this pharmacokinetic analysis for consecutive times: 5 min, 15 min, 30 min, 1 h, 2 h, 4 h, 8 h, 16 h and 24 h after the IP injection of ILA; n = 3 per time point. After treatment, mice were sacrificed, and plasma, skeletal muscle, cardiac muscle, liver and brain were collected.

All the pharmacokinetic parameters were estimated from the mean concentration values determined at each time point, and were evaluated by a non compartmental analysis using PKSolver (Version 2.0).

2.9. Muscle injury and in vivo treatment with ILA

The 4-month-old dystrophic mice were anesthetized by using 2% inhaled isoflurane and injected with 50 μL of cardiotoxin (CTX) (Sigma-Aldrich, 217503) in each tibialis anterioris (TA) muscle. At the same time and for the next 6 days, mice were treated with 100 mg/kg of ILA injected IP. The negative control mice were injected IP with the vehicle in which ILA was dissolved: 10% DMSO and 40% cyclodextrin solution. Mice were sacrificed on day 3 and 15 post CTX injury for the histological analysis, and on day 30 for the strength (Inverted Screen Test) and resistance (Treadmill test) tests. Mice weight and organs morphology/appearance was respectively evaluated during treatment and sacrifice.

2.10. Exercise-tolerance test

The Inverted Screen Test devised by Kondziela [40] was used to evaluate tolerance by placing a mouse in the center of a 43 cm^2 wire mesh consisting of 12 mm^2 of 1 mm diameter wire, surrounded by 4-cm deep wooden beading. Then a stopclock was started and the screen was rotated to an inverted position 40–50 cm above a padded surface. The time it took for the mouse to fall off was noted.

Finally, an exhaustion treadmill trial was performed to evaluate mice endurance of fusing a motorized treadmill (Panlab, model LE 8710 R), equipped with a socker plate as described previously [19,41,42]. The treadmill was run at 0º of inclination at 5 m/min for 5 min. Subsequently, speed was increased 1 m/min every minute. The test ended when the mouse remained more than 20 s on the shocker plate.

2.11. Muscle collection and processing

For tissue collection, mice were sacrificed on day 3 and 15 post CTX injury by cervical dislocation. The TA from mice were collected and frozen in liquid nitrogen-cooled isopentane. For the histological analysis, tissue specimens were sliced using a cryostat microtome (Leica, CM1510S) to 8 μm thick and mounted onto SuperFrost Ultra Plus Adhesion Slides (Thermo Scientific, J3800AMNZ).

2.12. Staining

For immunocytochemistry, the Sol8, wild-type and dystrophic-mice myoblasts were seeded in 24 well/plates and grown under differentiation conditions with ILA treatment on coverslips, which had been previously treated with 0.1 mg/mL Poly-L-Lysine solution (Sigma, P4832). Cells were fixed with 4% paraformaldehyde (PFA), permeabilized with PBS-50 mM NH_4Cl and 0.2% Triton-X100, blocked with PBS-0.2% gelatin and incubated under humid conditions with anti-MF20 (Table 2) overnight at 4ºC. Subsequently, they were incubated in secondary antibody AlexaFlour® Goat Anti-rabbit 488 (Table 2) for half an hour at room temperature (RT) and in the dark. Finally, nuclei were counterstained and mounted with Prolong™ Diamond Antifade Mountant with DAPI Invitrogen (Thermo Fisher Scientific, P36966). Images were taken with a Leica TCS SPE LAS AF confocal microscope and quantifications were performed with the Leica Biosystems LasX program.

Table 2
Antibodies used for immunostaining.

Primary Antibody	Source	Concentration/ Dilution	Company	Identifier
Anti-MF20	Mouse	5 μg/mL	Developmental Studies Hybridoma Bank (DSHB)	RRID: AB_2147781
Anti-Ki67 (SP6)	Rabbit	1/250	Abcam	ab16667; RRID: AB_302459
Anti-MyoD1 (5.8 A)	Mouse	5 μg/mL	DAKO	M3512; RRID: AB_2148874
Anti-eMyHC (F1.652)	Mouse	5 μg/mL	Developmental Studies Hybridoma Bank (DSHB)	RRID: AB_528358
Anti-Laminin	Rabbit	5 μg/mL	Sigma-Aldrich	L9393; RRID: AB_477163
Secondary Antibody	**Source**	**Concentration/ Dilution**	**Company**	**Identifier**
AlexaFluor® 488	Goat Anti-mouse	1/200	Thermo Fisher Scientific	A-11001; RRID: AB_2534069
AlexaFluor® 633	Goat Anti-rabbit	1/200	Thermo Fisher Scientific	A-21071; RRID: AB_2535732

For immunohistochemistry, the cryosection samples were tempered and fixed in 4% PFA for 10 min at RT. In citrate buffer (10 mM sodium citrate, 0.05% Tween-20, pH 6.0) epitopes were unmasked in a pre-heated water bath at 96ºC for 30 min. Then samples were incubated first with TBS-BSAT (10 mM Tris, 0.9% NaOH, 0.02% sodium azide, 2% BSA, and 0.1% Triton-X100) for 30 min at RT and later with primary antibodies (listed in Table 2) overnight at 4ºC under humidity conditions. The next day, Alexa-Fluor-conjugated secondary antibodies (Table 2) were incubated for 2 h at RT. Finally, samples were counter-stained and mounted with Prolong™ Diamond Antifade Mountant with DAPI Invitrogen. Images were taken with a confocal microscope and quantifications were performed with the Leica Biosystems LasX program.

For hematoxilin-eosin (H&E) staining, cryosection samples were tempered and fixed with 4% PFA for 10 min at RT. Then samples were washed in water several times and incubated with Mayer's Hematoxylin solution (Sigma-Aldrich, MHS32) for 10 min until nuclei were stained. After incubation with Activated Eosin Y Solution 0'5% (Merck, 1098441000) for 10 min and several washes with water, samples were performed prior to dehydration. DPX (AppliChem Panreac, 255254. l1608) was used as the mounting medium. Images were captured with a 2.0-MP digital microscope camera, which was attached via a c-mount to the side port of a Motic AE2000 microscope.

For collagen staining, cryosection samples were tempered and hydrated with PBS 1 × for 2 min, and then stained at RT for 30 min with 0.2% Syrian red (BDH, 34149) in distilled water saturated with picric acid (AppliChem Panreac, 141048.1609), as described by Esteban et al. (2005). Afterward, samples were washed 3 times with distilled water and dehydrated in an increasing series of alcohols (50%, 70%, 96% and 100%), 1 min each. Sections were rinsed with 2 steps of xylol, 1 min each, and were finally mounted with DPX to be observed under polarized light microscopy.

2.13. Western blot assay

The total protein from the treated Sol8 myoblast, and from the wild-type and dystrophic-mice TA explants, was extracted using Cell Lysis Buffer (1X Cell Lysis Buffer (Cell Signaling, 9803 S), 1% Protease and

Phosphatase Inhibitor Cocktail (Sigma, PPC1010), and 1% Phosphatase Inhibitor Cocktail 2 (Sigma, P5726)), to be quantified by a BCA assay (Pierce™ BCA Protein Assay Kit, Thermo Scientific, 23227) using EnVision by PerkinElmer.

The extracted protein (10 μg/lane) was boiled for 5 min and mixed with Laemmli Sample Buffer, which was previously prepared with β-mercaptoethanol. The protein samples were loaded and separated in a 4–15% precast polyacrylamide gel and then transferred to PVDF membranes. Membranes were blocked with Fish Serum Blocking Buffer (Thermo Scientific, 37527) for 1 h at 37ºC and incubated overnight at 4ºC with the primary antibodies listed in Table 3. After washing with PBS-T, membranes were incubated for 1 h at 37ºC with a secondary antibody (Table 3). All the antibodies were diluted in Fish Serum Blocking Buffer: PBS-Tween20 1:1. Immunoreactive bands were visualized and analyzed using a LI-COR Odyssey® imaging system. Quantification was performed by the ImageJ2 software (FIJI Version 2.14.0/1.54 f).

2.14. RT-qPCR analysis

In order to extract the total RNA from the treated cells, the ReliaPrep RNA Cell Miniprep System" (Promega, Z6011) was used following the instructions described in the protocol. For the total RNA extraction from the treated muscle explants, "Direct-zol RNA Miniprep" (Zymo Research, R2051) was used following the instructions described in the protocol. The total RNA concentration of each sample was quantified by Thermo Fisher Scientific NanoDrop 2000 using 1.5 μL per sample.

mRNA was retro-transcribed from 500 ng of the previously extracted total RNA using the "Maxima First Strand cDNA Synthesis kit for RT-qPCR" (Thermo Fisher Scientific, K1642) in a thermocycler (Bio-Rad C1000 Touch™ Thermal Cycler) in line with the manufacturer's instructions. Finally, the obtained cDNA was diluted 1:5.

The mRNA expression levels were quantified by real-time semi-quantitative PCR (RT-qPCR) from 1 μL of the diluted cDNA obtained from the retro-transcription reaction following the protocol of the Sso-Fast™ EvaGreen® Supermix kit (Biorad, 1725202). RT-qPCR was performed by a CFX Connect Real-Time PCR Detection System (Bio-Rad Laboratories). The qPCR program consisted of 95ºC for 30 s (initial denaturalization), followed by 40 cycles of 95ºC for 5 s (denaturalization); 60ºC for 10 s (annealing) and 75ºC for 7 s (extension). Finally, melt curves were determined by an initial step of 9ºC for 5 s, followed by 0.5ºC increments for 7 s from 65ºC to 95ºC. The relative level of each gene expression was which indicates its suitability as a reference gene). The primers used for mRNA qPCR are listed in Table 4.

2.15. Statistical analysis

All the statistical analyses were conducted with GraphPad Prism (version 9.5.0 of the GraphPad software, LLC). Data were obtained from the independent experiments performed in triplicate. They are presented as mean±standard deviation. Differences between two groups were analyzed by the unpaired Student's t test.

Table 3
Antibodies used for Western Blot.

Primary Antibody	Source	Dilution	Company	Identifier
GAPDH	Rabbit	1/40,000	Cell Signalling	5174 (D16H11)
α/β-TUBULIN	Rabbit	1/1000	Cell Signalling	2148
β-CATENIN	Rabbit	1/1000	Cell Signalling	9562
Non-phospho (Active) β-CATENIN	Rabbit	1/1000	Cell Signalling	8814 (D13A1)
GSK-3β	Rabbit	1/1000	Cell Signalling	12456 (D5C5Z)
Phospho GSK-3β (Ser9)	Rabbit	1/1000	Cell Signalling	5558 (D85E12)
Secondary Antibody	**Source**	**Dilution**	**Company**	**Identifier**
IgG Alexa Fluor Plus 488	Goat anti-Rabbit	1/10,000	Invitrogen	SA5-35571

3. Results

3.1. ILA-mediated GSK-3β inhibition promotes the myogenic differentiation of myoblasts and muscle stem cells

It has been shown that the GSK-3β-mediated modulation of the canonical Wnt/β-Catenin pathway plays fundamental roles in myogenic differentiation during embryonic and adult myogenesis [27–29]. Indeed Wnt signaling induces GSK-3β inactivation that leads to β-CATENIN stabilization and activation. While the non activated β-CATENIN is degraded in the cytoplasm, the activated β-CATENIN enters the nucleus and is required to coordinate the activation of myogenic genes for a successful differentiation of myoblast and MuSCs during muscle regeneration [43,44]. As the ability of ILA to inhibit GSK-3β activity has been previously reported in the neuroblastoma cell line [33], and as GSK-3β inactivation leads to β-CATENIN activation, here we first checked if the ability of the compound ILA to inhibit GSK-3β activity could increase the myogenic differentiation of myoblasts. To check this, Sol8 cells, a myoblast cell line [45], were cultured with different ILA doses, which have shown good effectiveness in inhibiting GSK-3β in other cell types [33]. After 3 days in differentiation medium, we observed that the number of differentiating $MF20^{pos}$ myoblasts was enhanced in the ILA-treated cells compared to the control and in a dose-dependent manner (Fig. 1B-C). We also found a significant increase in the fusion index after ILA treatment (Fig. 1B-C). These findings indicate that ILA increases the capability of Sol8 myoblasts to form myotubes.

To further mechanistically explore the effects of ILA treatment on myoblasts, the levels of inactivated GSK-3β and activated β-CATENIN were evaluated by a Western blot in the ILA-treated myoblasts after 24 h of ILA compound administration. This analysis revealed a non-significant trend to increase the inactive GSK-3β/total GSK-3β proteins ratio in the cultured cells treated at both ILA doses (Fig. 1D). The increase in the amount of active β-CATENIN/total β-CATENIN in the treated cells in a dose dependent manner was noteworthy (Fig. 1D). Moreover, the RT-qPCR analyses showed an increase in the transcript levels of the β-CATENIN target genes, such as *Myod1* and *Myogenin* (Fig. 1E). These results suggest that GSK-3β inhibition mediated by ILA treatment modifies the in vitro cell differentiation potential of myoblasts by increasing β-Catenin signaling.

As the myogenic differentiation of MuSCs is essential for regenerating and maintaining muscle mass, the effects of ILA treatment on the myogenic progression of MuSCs and hMuSCs were also evaluated. To address this, the freshly isolated cells from tibialis anterioris muscle (TA) of the 4-month-old mice were treated with ILA during in vitro differentiation. As shown in Fig. 2A, after 8 days of culture in the differentiation medium, the number of formed $MF20^{pos}$ cells was clearly enhanced in the treated mouse MuSCs compared to the control. We noted that, although the number of $MF20^{pos}$ cells significantly increased at both the assayed ILA doses versus the control, the number of differentiating cells was 4- and 2-fold higher in the cell cultures treated with 25 and 50 μM ILA, respectively. We next tested if ILA also acted the in hMuSCs isolated from human muscle. Thus the freshly isolated hMuSCs from muscle biopsies were treated with the same ILA doses and the effects of treatment during in vitro differentiation were evaluated by myotube number and length quantification on day 8 of culture in differentiation medium. As observed in Fig. 2B, and similarly to what occurred in mouse cells, the number of myotubes was significantly higher in the hMuSCs treated with the 25 μM dose of ILA and myotube length was longer at both the assayed doses. Collectively, these data reveal ILA's capability to also boost the myogenic potential of mouse and human stem cells.

Table 4
The primers used for mRNA qPCR.

Gene	Organism	Forward Primer (5' to 3')	Reverse Primer (5' to 3')
Gusb (NM_010368.2)	*Mus musculus*	ACGCATCAGAAGCCGATTAT	ACTCTCAGCGGTGACTGGTT
Myod1 (NM_010866.2)	*Mus musculus*	GGCTACGACACCGCCTACTA	TCCCTGTTCTGTGTCGCTTA
Myog (NM_031189.2)	*Mus musculus*	CTACAGGCCTTGCTCAGCTC	ACGATGGACGTAAGGGAGTG
Tnf-a (NM_013693.3)	*Mus musculus*	TCTACTGAACTTCGGGGTGA	AGGGTCTGGGCCATAGAACT
IL-1b (NM_008361.4)	*Mus musculus*	GGGCCTCAAAGGAAAGAATC	CTTCTTTGGGTATTGCTTGG
IL-6 (NM_031168.2)	*Mus musculus*	GATGGATGCTACCAAACTGGA	GGTACTCCAGAAGACCAGAGGA
Mcp-1 (NM_011333.3)	*Mus musculus*	AAGAGGATCACCAGCAGCAG	TCTGGACCCATTCCTTCTTG

3.2. GSK-3β/Beta-Catenin pathway is altered in mdx dystrophic mice muscle and ILA enhances the myofiber formation of dystrophic muscle stem cells

In muscle degenerative diseases like DMD, previous works in our laboratory have pointed out that dystrophic MuSCs exhibit limited myogenic differentiation capability [19,42]. As β-Catenin signaling is essential for proper SC myogenic differentiation, and as GSK-3β activity regulates β-CATENIN activation/stabilization in skeletal muscle [44,46,47], we wondered if the ILA-mediated capability for GSK-3β inhibition and β-CATENIN activation would modulate the myogenic potential of dystrophic MuSCs. To check this, we used dystrophic mdx mice, a well-characterized mouse model for DMD [48]. First, the basal levels of GSK-3β activity and the β-CATENIN protein were examined in the muscles of this mouse model. Interestingly, the Western blot analyses in the TA muscles isolated from the 4-month-old dystrophic mice revealed that, whereas no changes in GSK-3β inactivated form were detected, a significant increment in the total GSK-3β (activated GSK-3β + inactivated GSK-3β forms) occurred in dystrophic muscles compared to the control wild-type (Fig. 3A). This finding, together with the fact that the dystrophic mdx mice muscles displayed a lower GSK-3β inactivated/total GSK-3β ratio (Fig. 3A), suggest that the increased of total GSK-3β levels were due mainly to the GSK-3β activated form in this context. As a consequence, the β-CATENIN protein levels also lowered, which indicates a higher degradation rate mediated by GSK-3β activity (Fig. 3A). These results suggest that the canonical WNT/β-Catenin pathway could be attenuated in dystrophic mice due to altered GSK-3β action.

As ILA is an inhibitor of GSK-3β, and as we found that it modulated myogenic differentiation by increasing β-Catenin signaling, we next investigated its ability to modulate the myogenic potential of dystrophic MuSCs. For that purpose, the freshly isolated MuSCs from the TA of the 4-month-old dystrophic mice were cultured and treated with different ILA doses. The myogenic potential in vitro of the dystrophic MuSCs treated with ILA was evaluated by MF20 staining. As observed in Fig. 3B, the dystrophic MuSCs cultured for 8 days in differentiation medium at varying ILA concentrations displayed a significantly bigger amount of differentiating $MF20^{pos}$ cells at the 25 μM dose and this effect is maintained when the dose was increased to 50 μM (Fig. 3B). Therefore, these findings point out that ILA enhances the capability of dystrophic MuSCs to reach myogenic differentiation and to form myotubes, and they suggest that ILA administration can be proposed to increase muscle regeneration in a dystrophic context.

3.3. Acute toxicity and pharmacokinetic analysis

Drug-drug interaction was performed by evaluating drug metabolism via the cytochrome P450 system. Cytochrome P450 enzymes are required for the detoxification of foreign chemicals and are mediators of drug interactions, so new agents must undergo extensive drug interaction studies before they reach the clinic [37]. The three main isoforms of cytochrome P450 were evaluated. The data showed that ILA does not inhibit CYP3A4, CYP2D6 and CYP2C9 (IC_{50} >40 μM). Control inhibitors showed: CYP3A4 inhibitor ketokonazol, IC_{50} = 0.038[0.034–0.042] μM; CYP2D6 inhibitor sulfaphenazole, IC_{50} = 0.46[0.36–0.59] μM; CYP2D6 inhibitor quinidine, IC_{50} = 0.24[0.18–0.33] μM. The results obtained indicate a low probability of pharmacologic interaction and support their use for combined therapy.

In vitro cardiotoxicity was assayed by testing the inhibitory effect of that ILA on the potassium (hERG), calcium (Cav1.2) and sodium (Nav1.5) channels in a cellular heterologous expression system. The risk of cardiotoxicity is one of the main adverse effects of drugs that must be controlled in the early stages of preclinical drug development [49]. The results showed that isolecanoric acid had no effect on the inward rectifying potassium, calcium and sodium ion channels at the maximum concentrations tested of 50 μM (control inhibitors showed: hERG inhibitor astemizole, IC_{50} = 0.65[0.57–0.75] μM; Cav1.2 inhibitor israpidin, IC_{50} = 0.009[0.0006–0.014] μM, and Nav1.5 inhibitor tetrodotoxin, IC_{50} = 2.8[2.3–3.5] μM.

In addition, the mutagenic potential of ILA was assayed by the AMES test. A commercial kit, based on the most common bacterial reverse-mutation test, known as the "Ames Test" [50], was used to evaluate the mutagenicity of isolecanoric acid. The results showed that ILA does not show mutagenic potential.

To evaluate in vivo acute toxicity, ILA IP injection was performed at 250, 150 and 100 mg/kg in the wild-type mice. The results showed that no marked changes in behavioral and physiological parameters were observed. In addition, mortality was not noticed during the 14 days of ILA administration.

To further evaluate the pharmacokinetic of ILA, a single dose of 100 mg/kg injected IP was tested in mice. The plasma and the tissue concentrations of the compound were determined by the LC-MS/MS method described in the Supplementary Material. The mean plasma concentration–time profile is represented in Fig. 4A. The main pharmacokinetic parameters are compiled in Fig. 4B. The maximum concentration reached in plasma (Cmax) was 67.9 μg/mL± 3.6 μg/mL at 5 min, which represented 2.72% of the administered dose (Fig. 4A-B). The plasma drug concentration was detectable up to 24 h after ILA administration (Fig. 4A-B). The half-life time was 138.3 min and the $AUC_{0–1440}$ / $AUC_{0-\infty}$ ratio was (0.9996). These results would allow administration every 24 h (Fig. 4A-B).

With the IP injection of 100 mg/kg of ILA into dystrophic mice, there were no significant changes in the body weight of the ILA-treated group compared to the vehicle-treated group (Fig. S1A). ILA administration in vivo did not impact the organ macromorphology of the dystrophic mice after sacrifice on post-treatment days 3, 15 and 30 (Fig. S1B).

ILA was also evaluated in different tissues. Fig. S1C shows the drug concentration for several analysis times and the Cmax, Tmax and t1/2

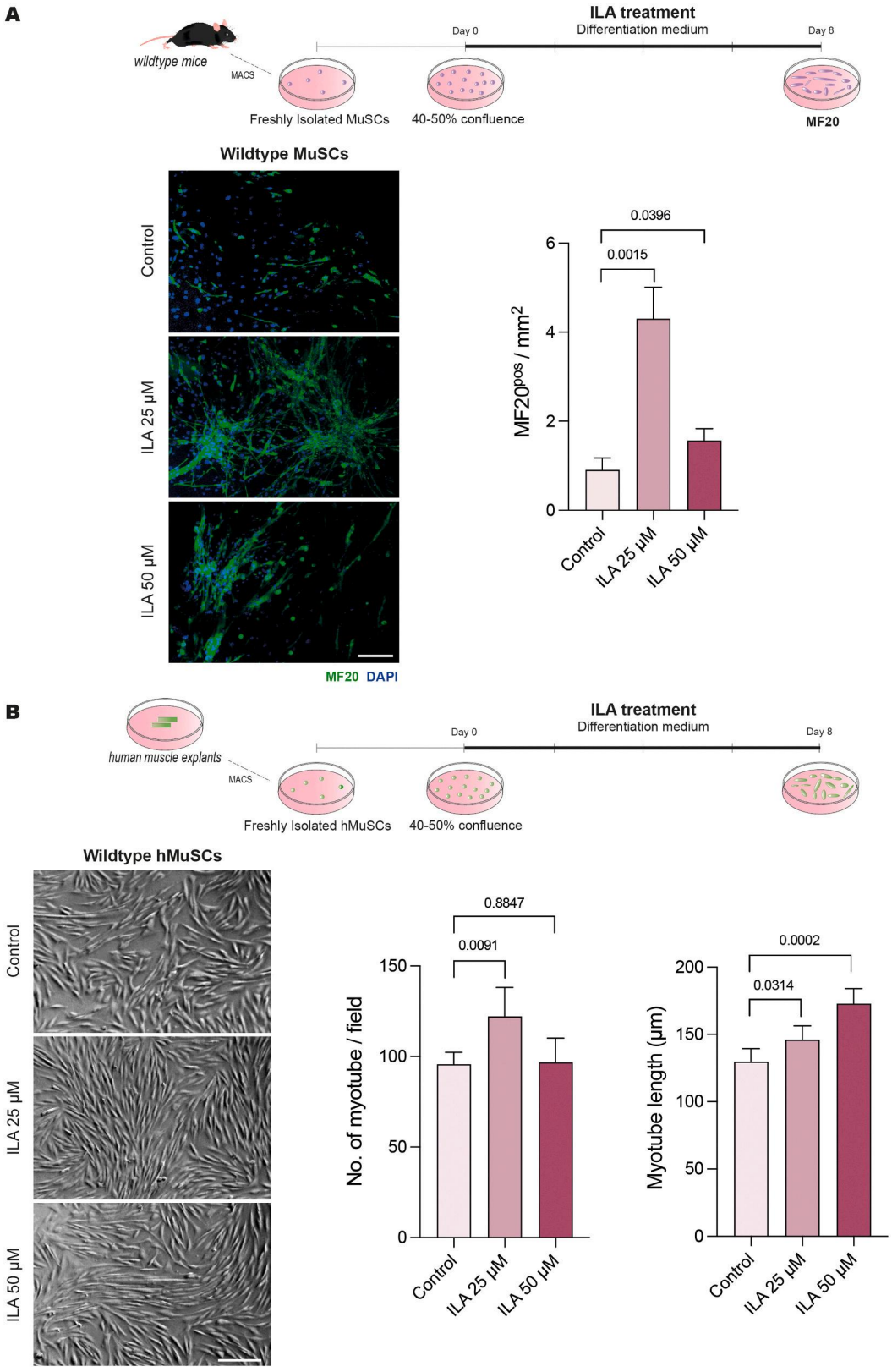

Fig. 2. ILA treatment enhances myogenic differentiation of MuSCs and hMuSCs. (A) Scheme of ILA treatment in freshly isolated wild-type MuSCs and representative images of MF20 staining in the MuSCs treated at different ILA doses of ILA; quantification of the number of MF20pos cells per area is shown (n = 3 mice and 3 independent experiments per mice, 5 aleatory fields per condition). Scale bar: 100 µm. MuSCs, muscle stem cells. (B) Scheme of ILA treatment in the freshly isolated hMuSCs and representative images of the hMuSCs treated at different ILA doses; quantification of the number of myotubes/field and myotubes length in hMusSCs cultures after ILA treatment is shown (n = 3 independent experiments, 5 aleatory fields per condition). Scale bar: 200 µm. hMuSCs, human muscle stem cells.

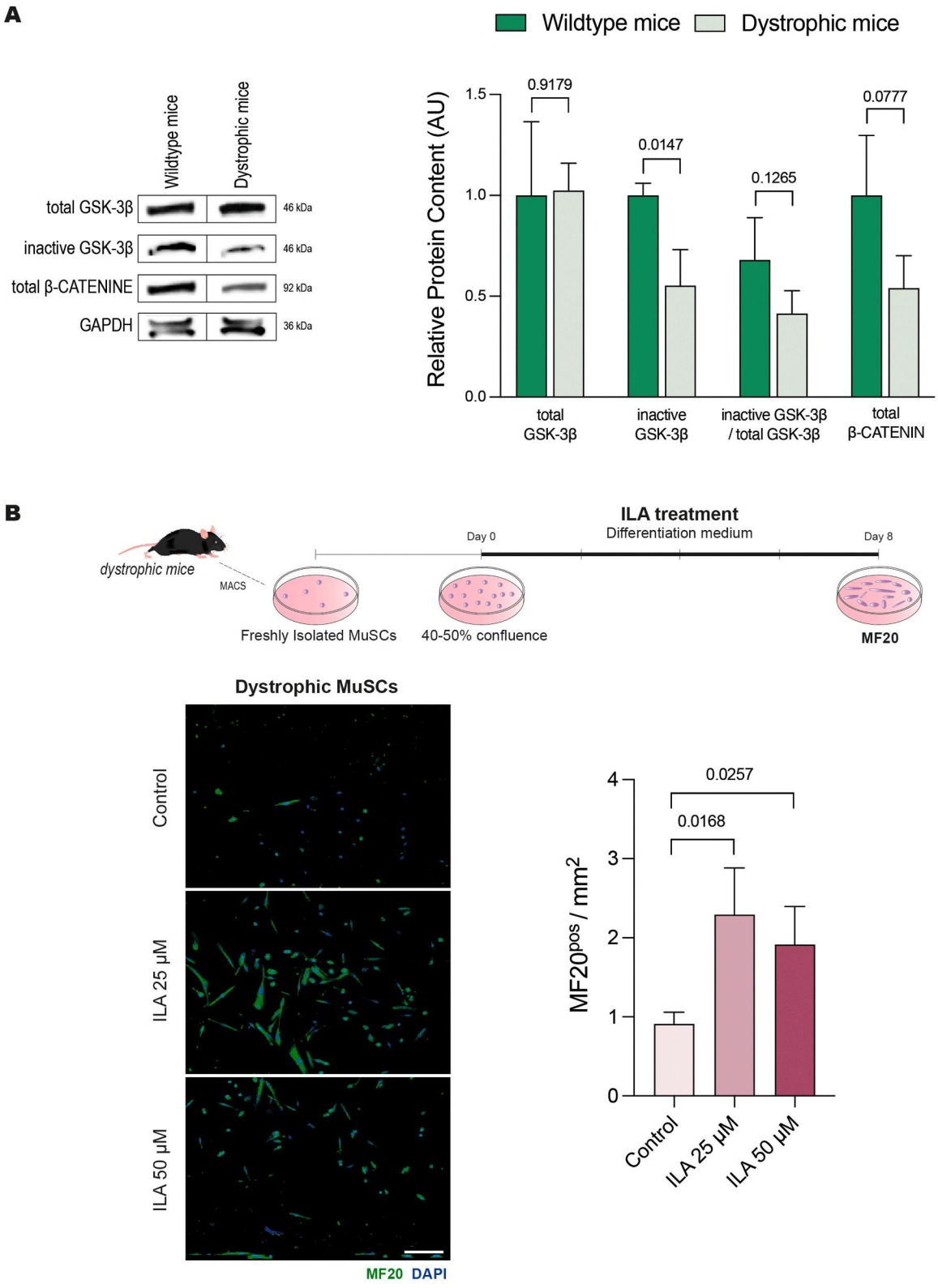

Fig. 3. Inactivated GSK-3β and β-CATENINE are altered in dystrophic muscles and ILA treatment enhances the myogenic potential of dystrophic MuSCs. (A) Representative Western blot of the total GSK-3β, inactive GSK-3β and total β-CATENINE, and the relative quantification for the protein content of the total GSK-3β; inactive GSK-3β; inactive GSK-3β versus the total GSK-3β; the total β-CATENINE in the TA muscles of the wild-type mice versus the dystrophic mice. GAPDH was used for total protein normalization (n = 2 wild type mice, n = 3 dystrophic mice). (B) Scheme of ILA treatment in the freshly isolated dystrophic mouse muscle SCs (MuSCS) and representative images of MF20 staining in dystrophic mouse MuSCS treated at different ILA doses; quantification of the number of $MF20^{pos}$ cells per area is shown (n = 3 mice and 3 independent experiments per mice, 5 aleatory fields per condition). Scale bar: 100 µm. MACS, magnetic cell isolation.

A

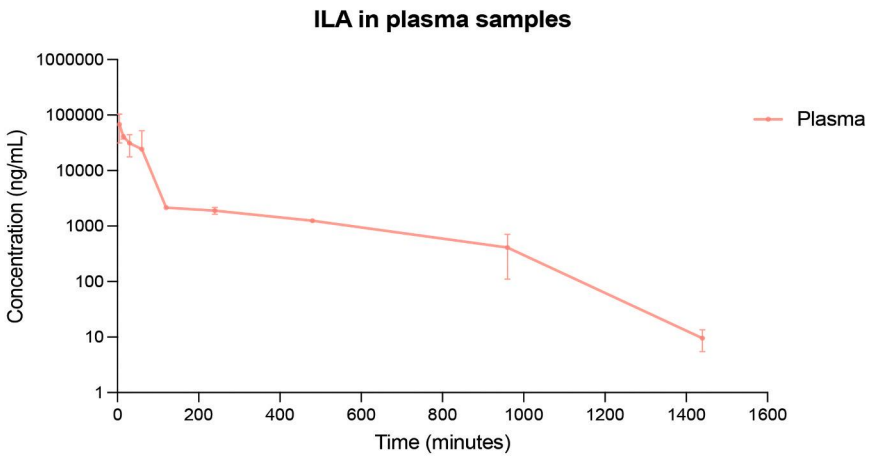

B

Pharmacokinetics parameters	Average ± SD
C_{max} (ng/mL)	67867 ± 3556.95
T_{max} (min)	5
$t_{1/2\beta}$ (min)	138.28 ± 8.10
$AUC_{0\text{-}1440}$	4211623 ± 2173802.28
$AUC_{0\text{-}\infty}$	4213518 ± 2174357.68

Fig. 4. Pharmacokinetic analysis of the ILA compound in the plasma extracted from the treated wild-type mice. N = 27 wild-type mice aged 4 months were randomized into nine groups for the pharmacokinetic analysis: 5 min, 15 min, 30 min, 1 h, 2 h, 4 h, 8 h, 16 h and 24 h after the IP injection of ILA; n = 3 per time point. (A) Plasma concentration of ILA at different times after IP administration of 100 mg/kg. (B) Basic pharmacokinetic parameters for ILA in the plasma samples are represented in the table. C_{max}: the maximum observed concentration; T_{max}: the time of the maximum observed concentration; $t_{1/2\beta}$: terminal elimination half-life; AUC_{0-1440}: area under the curve from zero to the last sampling time; $AUC_{0\text{-}\infty}$: area under the curve from zero extrapolated to infinity.

values of the drug in the analyzed tissues. The drug was detected in the liver, cardiac muscle and skeletal muscle for up to 16 h. In the brain, it was detected at a much lower concentration, with the last detection time being 8 h. The skeletal muscle/plasma concentrations ratio remained constant (approximately 9%; Fig. S1 A). These results demonstrate that ILA can penetrate the blood-brain barrier, but at a lower percentage compared to other tissues and organs.

3.4. *ILA treatment boosts muscle regeneration in the mdx dystrophic mice*

In order to address whether ILA treatment could modulate muscle regeneration in dystrophic mice, the TA of the 4-month-old dystrophic mice were injected with CTX, and mice were systemically IP treated with an ILA dose (100 mg/kg) daily for 7 days after the CTX injection (Fig. 5A). First, we evaluated the effects of ILA treatment on the generation of myogenic cells after MuSCs activation during early muscle regeneration. We observed that the in vivo administration of the compound increased the number of proliferating $KI67^{pos}$/$MYOD1^{pos}$ cells 3 days after the CTX injection (Fig. 5B). These findings suggest that ILA treatment enhances the functional ability of dystrophic MuSCs to activate and participate in tissue repair.

We also tested tissue regeneration by analyzing the newly formed myofibers by using an eMyHC antibody on day 3 of the CTX injection. As observed in Fig. 5C, the number of $eMyHC^{pos}$ myofibers was enhanced in the ILA-treated muscles. In addition, the histological analysis of the TA from dystrophic mice on 15 post-treatment days clearly showed a higher percentage of fibers with centralized nuclei (Fig. 5D), which revealed an increase in fusogenic myoblasts for regenerating myofibers. These findings indicate that the regenerative potential was enhanced in the dystrophic MuSCs after ILA treatment.

Functional performance was assayed in the ILA-treated dystrophic mice by the Inverted Screen Hanging Test, used to assess muscle stamina. The Treadmill Test until exhaustion was applied to evaluate muscle fatigue 30 days after muscle injury. The Inverted Screen Test showed that the hanging time significantly increased in the dystrophic mice treated with ILA compared to the control (Fig. 5E). In addition, the treadmill test revealed that the running distance was around 30% longer in the ILA-treated mice compared to the control, which indicates that compound administration boosts physical performance. Together, these results demonstrate that ILA treatment enhances muscle regeneration in dystrophic mice.

3.5. *ILA induces a decreased inflammatory response in muscle explants and mdx-macrophages*

In DMD, muscle degeneration is associated with the continuous activation of the innate immune system and the associated inflammatory response, which lead to chronic inflammation and, thus, causes additional tissue damage [51]. Therefore, treatments that modulate the inflammatory response are critical for restoring muscle stability and function.

GSK-3β has been recently identified as a potent regulator of the immune response, which leads to a proinflammatory response by activating the expression of pro-inflammatory genes, including chemokines and cytokines like tumor necrosis factor alpha (TNF-α), interleukin 6 (IL6), interleukin 1b (IL-1b) and Monocyte chemoattractant protein-1 (MCP-1) [52]. We then wondered if ILA-mediated GSK-3β inhibitory affects would also impact the inflammatory response in muscle. To check this, the cultured muscle explants of hindlimb muscles isolated from the 4-month-old wild-type mice were first treated with different ILA compound doses. An acute inflammatory response was induced by adding to culture medium lipopolysaccharide (LPS), a potent activator of acute inflammation [53]. The LPS-induced muscle explants were then treated with different ILA doses, and the expression of inflammatory cytokines TNF-α, IL-1b and MCP-1 were analyzed by RT-qPCR. As shown in Fig. 6A, LPS induction clearly increased the expression levels of

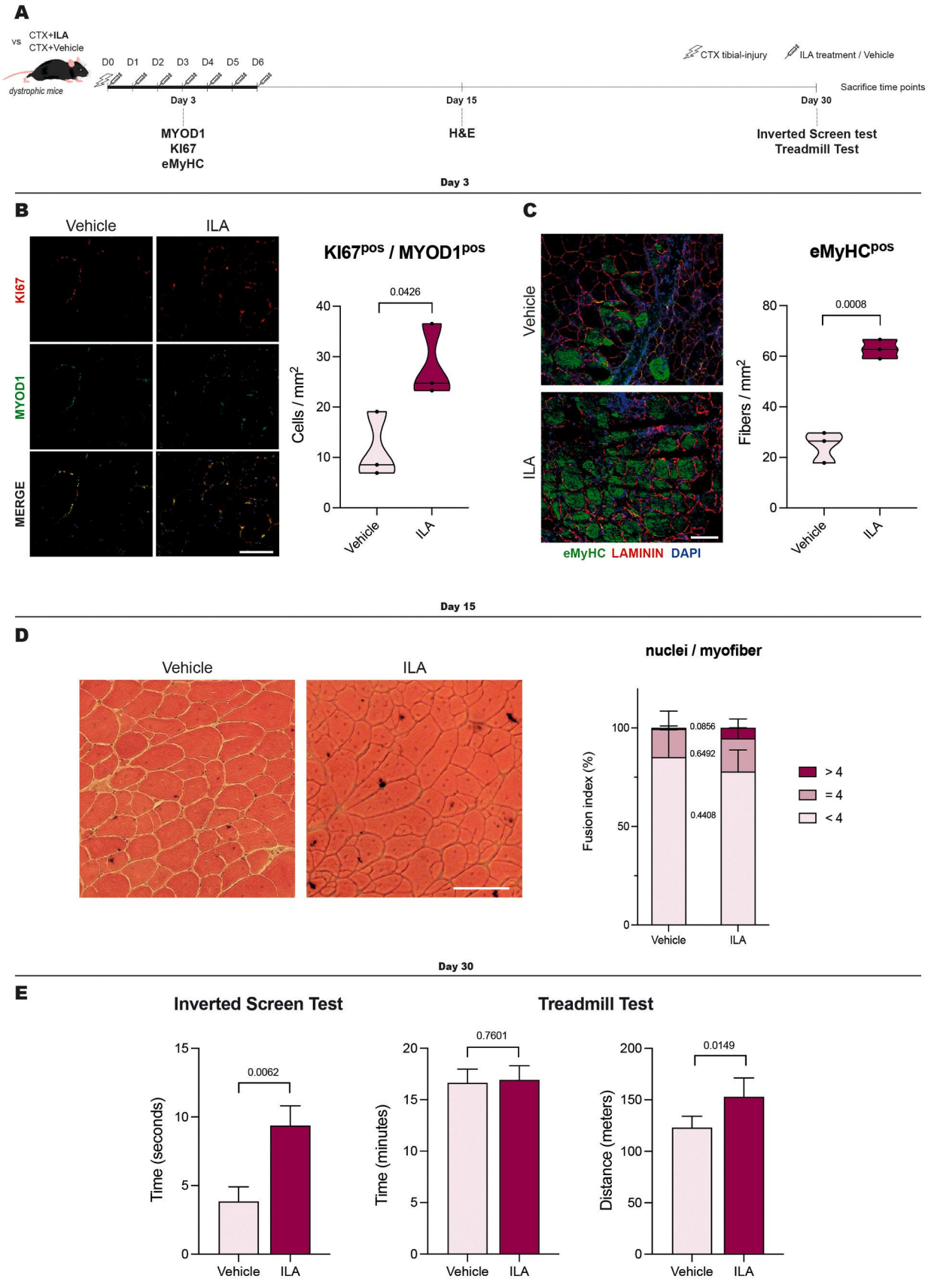

(caption on next page)

Fig. 5. ILA enhances muscle regeneration in dystrophic mice. N = 20 dystrophic mice, aged 4 months, were randomized into three groups for the muscle regeneration analysis: day 3 and day 15 after the intramuscular injections for the immune- and histochemical analyses (n = 3 per time point and condition), and day 30 after the intramuscular injections for functional tests (n = 4 per time point and condition). (A) Scheme of the CTX injection in TA muscle and IP administration of either ILA (100 mg/kg) or vehicle (control) in dystrophic mice. Scale bar: 50 μm. (B) KI67 and MYOD1 immunostaining in the cryosections from the ILA-treated and control TA muscles (3 post-administration days); quantification of the percentage of the $KI67^{pos}/MYOD1^{pos}$ cells is shown. Scale bar:100 μm. (C) eMyHC staining in the cryosections from the ILA-treated and control TA muscles (3 post-administration days); quantification of the number of the $eMyHC^{pos}$ myofibers per area is shown. Scale bar:100 μm. (D) H&E staining in the sections from the ILA-treated and control TA muscles (15 post-administration days) and the fusion index is shown. (E) The Inverted Screen Test and the Treadmill Test in the control and ILA-treated dystrophic mice (30 post-administration days).

TNF-α, IL-6, IL-1b and MCP-1 in the muscle explants. However, ILA treatment significantly decreased the expression of those proinflammatory cytokines with a dose-dependent response.

Given that the persistent release of cytokines, such as TNF-α, IL-1b and IL-6, by infiltrating macrophages is the major contributor to chronic inflammation in DMD [54], we decided to further explore if ILA treatment also affected macrophages-dependent cytokine production in a dystrophic context. Thus the monocyte-derived macrophages were isolated from dystrophic mice and treated with ILA at doses of 25 and 50 μM (Fig. 6B). One major finding was that the expression levels of TNF-α, IL-1b and IL-6 similarly decreased in the ILA-treated macrophages isolated from dystrophic mice (Fig. 6B). Altogether, these findings indicate that ILA treatment also ameliorates the pro-inflammatory response in a dystrophic context.

Finally, to address whether ILA mediated inflammatory response modulation targets fibrosis, muscle fibrosis was evaluated by Picrosirius staining after muscle injury and ILA treatment in dystrophic mice. As illustrated in Fig. 6C, Picrosirius staining reduced in the ILA-treated dystrophic mice after 15 days of muscle injury, which suggests that a decreased inflammatory response induced by ILA treatment would lead to mitigate fibrosis in dystrophic mice after muscle damage.

4. Discussion

DMD is a severe progressive, X-linked, neuromuscular disorder caused by mutations in the *dystrophin* gene. In DMD, lack of functional dystrophin protein makes the muscle membrane fragile, which leaves muscle fibers prone to damage during contraction. Muscle degeneration in DMD patients is closely associated with a prolonged inflammatory response, and although this is important for stimulating regeneration, inflammation is also thought to exacerbate muscle damage [20]. Several recent pieces of evidence have pointed out that DMD is a multifactorial disease in which muscle fiber weakness is associated with an adverse persistent inflammatory response and MuSCs' decreased myogenic capability [15,19,55,56]. Therefore, the development of new drugs that target this variety of factors might have a significant impact for DMD treatment.

Natural products and synthetically modified NP derivatives have successfully been developed for clinical use to treat human diseases in almost all therapeutic areas. Microbial natural metabolites represent one of the most important sources for the discovery of new drugs, with many drugs deriving from microbial metabolites having skillfully been introduced onto the pharmaceutical market [57]. In the past 20 years, the percentage of NPs or new NP-inspired chemical entities (NCEs) has risen to approximately 50% of all approved drugs [58]. Here we report that ILA, a natural product isolated from a fungal extract [33], increases the myogenic potential of dystrophic MuSCs by leading to boost dystrophic mice muscle regeneration, but also ameliorates the inflammatory response in a dystrophic context.

Synchronization of several steps involving exit from the cell cycle, migration to the site of damage, activation of the skeletal muscle-specific genes and cell fusion are essential for muscle regeneration, with myoblasts, the effector cells of muscle repair [59,60]. β-Catenin signaling is one of the most important pathways for embryonic muscle development and regeneration [26,44,61], and β-CATENIN activation mediated by GSK-3β inhibition improves myoblasts differentiation and fusion [30]. Here we show that the ILA compound, by acting as a GSK-3β inhibitor, increases the amount of active β-CATENIN in myoblasts by amplifying the myogenic gene transcription program and finally enhancing their myogenic differentiation potential. These results agree with the findings of Rudolf *et al.* (2016) [44], who showed that β-Catenin KO myoblasts contain a smaller amount of *Myod1* and *Myogenin* transcripts, by exhibiting a decreased differentiation potential, and the β-CATENIN function in adult myoblasts is crucial for their full regenerative potential.

In the muscle biology and performance context, it has been previously shown that GSK-3β inhibition enhances fatigue resistance in muscle via the nuclear factor of activated T-cells (NFAT) [62] and up-regulates skeletal muscle mitochondrial metabolism [63]. The in vivo deletion of GSK-3β accelerates muscle mass recovery in a disuse-induced muscle atrophy mouse model [64]. As the ILA compound acts by inhibiting GSK-3β activity, its administration might also have future applications to treat unmet medical needs that affect a broad sector of the world's population, such as muscle fatigue, atrophy and metabolic dysfunction, which are associated with chronic diseases, sarcopenia and cancer.

In the last few decades, several reports have pointed out that MuSCs in DMD dysfunctionally exhibit critical intrinsic defects, such as impaired asymmetric cell division, reduced myogenic commitment and altered differentiation kinetics [65]. Although recent research evidence has shown that restoring asymmetric cell division defects in MuSCs can have a tremendous therapeutic potential for DMD [19,65], the pharmacological modulation of other molecular pathways, such as SC-myogenic differentiation potential, has been less explored in this context. In light of this, it has been previously demonstrated that MuSCs require the canonical Wnt/β-catenin pathway for proper muscle regeneration [44]. In line with previous reports [66], we found that GSK-3β/β-Catenin signaling is altered in dystrophic muscles, and ILA-treatment, as a modulator of GSK-3β/β-Catenin activities, restores the myogenic potential of dystrophic MuSCs in vitro. More importantly, we also demonstrate that the in vivo administration of ILA enhances muscle regeneration in dystrophic mice, and improves muscle function and performance. Our findings stress that in vivo ILA administration does not lead to any sign of acute toxicity. As the ILA compound enhances myoblast differentiation, we conclude that ILA treatment in dystrophic mice acts mainly by incrementing myogenic differentiation. However, we also observe that ILA treatment increases the number of proliferating $KI67^{pos}/MYOD1^{pos}$ cells 3 days after CTX injection because β-CATENIN can also favor asymmetric divisions in embryonic stem cells [67] and dystrophic MuSCs fails to undergo proper asymmetric cells divisions, which generate myogenic $MyoD^{pos}$ precursors cells [59]. We cannot rule out the possibility that β-CATENIN effects on asymmetric divisions may contribute to the observed effects.In addition, as GSK-3β inhibition improves the pro-myogenic role of Fibro/Adipogenic Progenitors (FAPs), a critical cell type that mediates pro-myogenic signals and muscle regeneration [47], nor can we rule out that the effects mediated by ILA-GSK-3β inhibition in muscle can also modify FAPs behavior in this context. Overall, as loss of regenerative capability of MuSCs in muscular dystrophy pathologies exacerbates the pathology and the development of new therapies to promote muscle repair and regrowth are necessary, our results indicate that ILA could be proposed as a new therapeutic molecule to promote muscle regeneration in DMD.

In healthy muscles, muscle damage initiates inflammation and the recruitment of immune cells that secrete chemokines and cytokines,

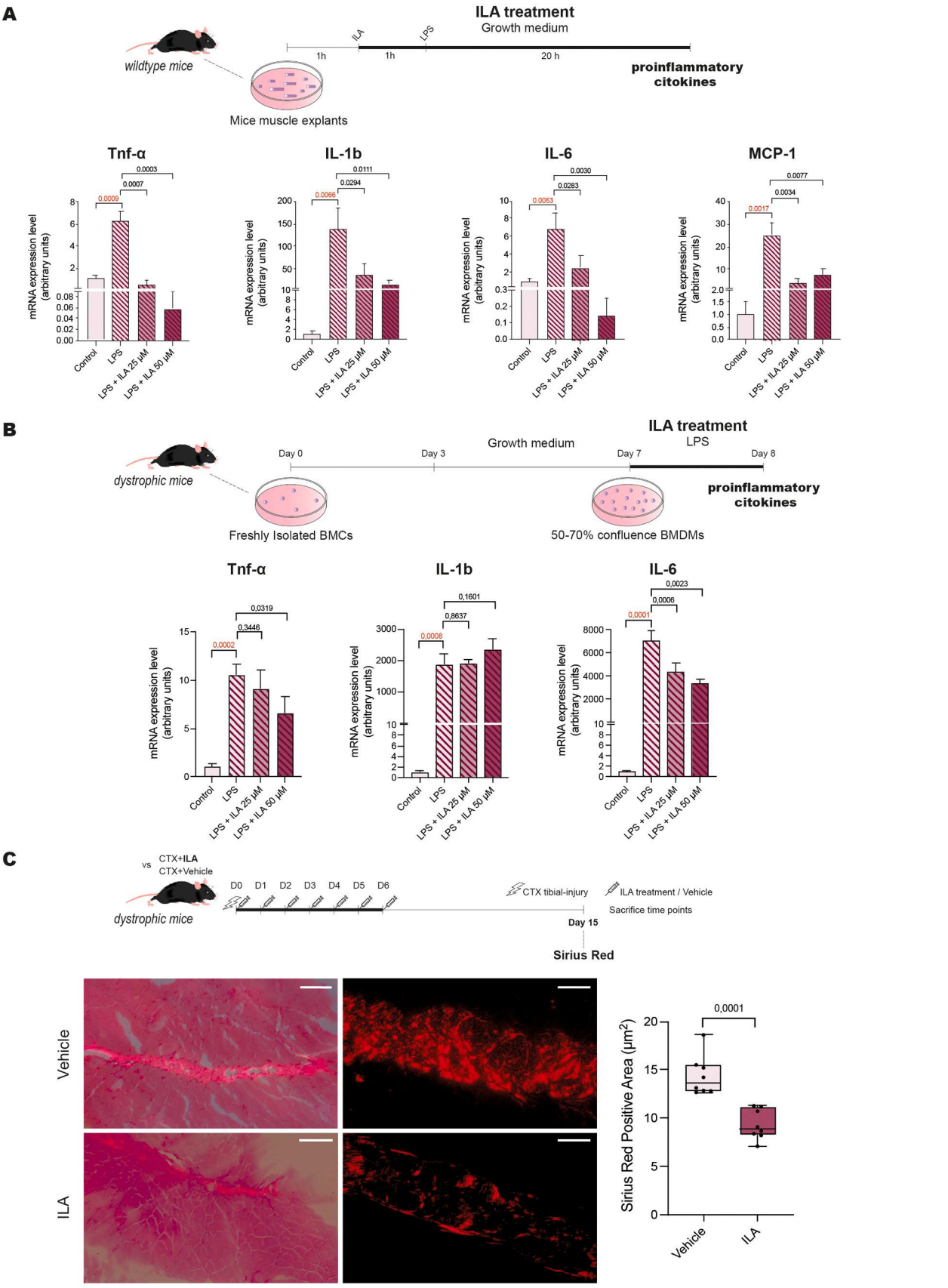

(caption on next page)

Fig. 6. Inflammatory response is reduced in both the muscle explants and bone marrow-derived macrophages (BMDMs) after ILA treatment. (A) Scheme of the wild-type mice muscle explants incubated with 10 μg/mL LPS in the absence or presence of 25 μM and 50 μM ILA treatment. The RT-qPCR analysis for TNF-a, IL-1b, IL-6 and Mcp-1 (n = 3 mice, 3 independent muscle explants were assayed per mice and condition). (B) Scheme of the bone marrow-derived macrophages (BMDMs) isolation, cultures and ILA treatment at different doses. The RT-qPCR of the gene expression of TNF-a, IL-1b and IL-6 is shown (n = 3 mice, 3 independent experiments were assayed per mice and condition). BMCs, bone marrow cells. BMDMs, bone marrow-derived macrophages (BMDMs). (C) Scheme of the CTX injection in TA muscle and IP administration of either ILA (100 mg/kg) or vehicle (control) in dystrophic mice (n = 3 mice per condition). Representative images of Picrosirius red staining in the TA muscles of dystrophic mice 15 days after CTX injection and ILA administration observed by Bright-field microscopy and linear polarization. Note that Sirius red-bound fibrillar collagens are bright red and in sharp contrast to the rest of the tissue, which remains black. The TA overview images (left) were obtained with a 4x magnification lens (scale bar: 200 μm) and higher magnification images (right) were obtained with a 20x magnification lens (scale bar: 30 μm). Quantification of the Sirius-Red positive area is shown.

which lead to a local inflammatory response. Initially, such immune system activation benefits tissue regeneration by inducing the proliferation and maturation of satellite cells. However, the persistent activation of the immune response in DMD leads to the permanent recruitment of M1 macrophages, which release proinflammatory cytokines like TNF-α, IL-6, IL-1β and MCP-1 by causing a chronic inflammatory condition that contributes to impaired muscle repair and disease exacerbation [68]. The most standard pharmacological treatment to suppress muscle inflammation in DMD is corticosteroids. However, because of insufficient therapeutic efficacy and considerable side effects, the development of more effective drugs in this context is necessary [69]. Seeing that GSK-3β controls proinflammatory cytokine production, the therapeutic use of small molecules and natural compounds that regulate GSK-3β activity to reduce the deleterious effects of the inflammatory response has been proposed [52]. We provide evidence that ILA, a GSK-3β inhibitor, decreases the expression of inflammatory cytokines TNF-α, IL-1b and MCP-1 in muscle explants after an inflammatory stimulus, which indicates that ILA ameliorates the inflammatory response in skeletal muscle. We also demonstrated that ILA treatment clearly reduces cytokine production in dystrophic macrophages. Those results, together with the fact that muscle fibrosis diminished in the ILA-treated dystrophic mice, led us to think that the ameliorated inflammation induced by ILA treatment could give rise to mitigate fibrosis in dystrophic mice.

In recent years, new therapies that target regenerative defects and chronic inflammatory response have been proposed [70]. Here we show, for the first time, that GSK-3β inhibition mediated by a natural compound (ILA) efficiently targets regeneration and inflammatory response, which are two adverse effects closely associated with DMD.

5. Conclusions

This study demonstrates that treatment with the natural ILA compound increases the myogenic potential of dystrophic MuSCs, and the in vivo ILA administration to dystrophic mice enhances muscle regeneration, force and the global physical function compared to untreated mice. Our findings further demonstrate that ILA treatment ameliorates the inflammatory response by decreasing cytokine production in dystrophic macrophages and reducing muscle fibrosis in dystrophic mice. Considering that DMD is a multifactorial disease caused by muscle fiber fragility, deleterious inflammatory environment and the reduced myogenesis capacity of MuSCs, ILA administration can be considered a highly efficient therapeutic option for DMD.

Ethics approval and consent to participate

The study was performed in accordance with the Code of Ethics of the World Medical Association (Declaration of Helsinki) for experiments involving humans. It was approved by the Ethics Committee at the University of Jaen and the Hospital Universitario Virgen de las Nieves from Granada, and by the Human Research Ethics Committee of the UGR. Informed consent was obtained from all the participants. All the animal experiments complied with the ARRIVE guidelines. They were carried out in accordance with EU Directive 2010/63/EU for animal experiments and were approved by the Ethics Committee at the University of Jaen.

Funding sources

This work was supported by the Duchenne Parent Project, Spain Foundation (grant number DUCHENNE_2018/001). Ministerio de Ciencia e Innovación, Gobierno de España (grant number PID2022–138163OB-C31). Consejeria de Universidad, Investigacion e Innovacion, Junta de Andalucia (grant number ProyExcel_00513).

CRediT authorship contribution statement

Montolio Marisol: Writing – review & editing. **Reyes Fernando:** Resources, Writing – review & editing. **Genilloud Olga:** Resources, Writing – review & editing. **González-Menéndez Victor:** Resources. **Crespo Gloria:** Resources. **Díaz Caridad:** Investigation, Resources. **Ramos Maria C:** Investigation, Writing – review & editing. **Rodriguez-Outeiriño Lara:** Formal analysis. **Sanchez-Fernandez Cristina:** Formal analysis. **Aránega Amelia:** Conceptualization, Funding acquisition, Supervision, Writing – original draft. **Matias-Valiente Lidia:** Formal analysis, Investigation. **Hernandez-Torres Francisco:** Conceptualization, Funding acquisition, Investigation, Writing – review & editing.

Declaration of Competing Interest

The authors declare that they have no known competing financial interests or personal relationships that could have appeared to influence the work reported in this paper.

Data availability

Data will be made available on request.

Acknowledgement

This work was partially supported by grants DUCHENNE_2018/001 (Duchenne Parent Project, Spain Foundation), PID2022–138163OB-C31 (Ministerio de Ciencia e Innovación, Gobierno de España) and ProyExcel_00513 (Consejeria de Universidad, Investigacion e Innovacion, Junta de Andalucia).

Data availability

All the data needed to support the conclusions are present in this paper. Nonetheless, any clarification about the support data will be made available upon request.

Appendix A. Supporting information

Supplementary data associated with this article can be found in the online version at doi:10.1016/j.biopha.2023.116056.

References

[1] J.R. Mendell, C. Shilling, N.D. Leslie, K.M. Flanigan, R. al-Dahhak, J. Gastier-Foster, K. Kneile, D.M. Dunn, B. Duval, A. Aoyagi, C. Hamil, M. Mahmoud, K. Roush, L. Bird, C. Rankin, H. Lilly, N. Street, R. Chandrasekar, R.B. Weiss, Evidence-based path to newborn screening for Duchenne muscular dystrophy, Ann. Neurol. 71 (2012) 304–313, https://doi.org/10.1002/ana.23528.

[2] N.P. Tavakoli, D. Gruber, N. Armstrong, W.K. Chung, B. Maloney, S. Park, J. Wynn, C. Koval-Burt, L. Verdade, D.H. Tegay, L.L. Cohen, N. Shapiro, A. Kennedy, G. Noritz, E. Ciafaloni, B. Weinberger, M. Ellington, C. Schleien, R. Spinazzola, S. Sood, A. Brower, M. Lloyd-Puryear, M. Caggana, Newborn screening for Duchenne muscular dystrophy: A two-year pilot study, Ann. Clin. Transl. Neurol. 10 (2023) 1383–1396, https://doi.org/10.1002/acn3.51829.

[3] S. Crisafulli, J. Sultana, A. Fontana, F. Salvo, S. Messina, G. Trifirò, Global epidemiology of Duchenne muscular dystrophy: an updated systematic review and meta-analysis, Orphanet J. Rare Dis. 15 (2020), 141, https://doi.org/10.1186/s13023-020-01430-8.

[4] A.E. Stark, Determinants of the incidence of Duchenne muscular dystrophy, Ann. Transl. Med 3 (2015) 287, https://doi.org/10.3978/j.issn.2305-5839.2015.10.45.

[5] E. Mercuri, F. Muntoni, Muscular dystrophies, Lancet Lond. Engl. 381 (2013) 845–860, https://doi.org/10.1016/S0140-6736(12)61897-2.

[6] D.G. Allen, O.L. Gervasio, E.W. Yeung, N.P. Whitehead, Calcium and the damage pathways in muscular dystrophy, Can. J. Physiol. Pharmacol. 88 (2010) 83–91, https://doi.org/10.1139/Y09-058.

[7] T. Saito, M. Kawai, E. Kimura, K. Ogata, T. Takahashi, M. Kobayashi, H. Takada, S. Kuru, T. Mikata, T. Matsumura, N. Yonemoto, H. Fujimura, S. Sakoda, Study of Duchenne muscular dystrophy long-term survivors aged 40 years and older living in specialized institutions in Japan, Neuromuscul. Disord. NMD 27 (2017) 107–114, https://doi.org/10.1016/j.nmd.2016.11.012.

[8] D.J. Birnkrant, K. Bushby, C.M. Bann, S.D. Apkon, A. Blackwell, D. Brumbaugh, L. E. Case, P.R. Clemens, S. Hadjiyannakis, S. Pandya, N. Street, J. Tomezsko, K. R. Wagner, L.M. Ward, D.R. Weber, DMD Care Considerations Working Group, Diagnosis and management of Duchenne muscular dystrophy, part 1: diagnosis, and neuromuscular, rehabilitation, endocrine, and gastrointestinal and nutritional management, Lancet Neurol. 17 (2018) 251–267, https://doi.org/10.1016/S1474-4422(18)30024-3.

[9] D.J. Birnkrant, K. Bushby, C.M. Bann, S.D. Apkon, A. Blackwell, M.K. Colvin, L. Cripe, A.R. Herron, A. Kennedy, K. Kinnett, J. Naprawa, G. Noritz, J. Poysky, N. Street, C.J. Trout, D.R. Weber, L.M. Ward, DMD Care Considerations Working Group, Diagnosis and management of Duchenne muscular dystrophy, part 3: primary care, emergency management, psychosocial care, and transitions of care across the lifespan, Lancet Neurol. 17 (2018) 445–455, https://doi.org/10.1016/S1474-4422(18)30026-7.

[10] H.V. Ruiten, K. Bushby, M. Guglieri, State-Of-The-Art Advances in Duchenne Muscular Dystrophy, EMJ Neurol. 21 2017. 2 (2017) 90–99, https://doi.org/10.33590/emj/10311993.

[11] R. Kayali, F. Bury, M. Ballard, C. Bertoni, Site-directed gene repair of the dystrophin gene mediated by PNA-ssODNs, Hum. Mol. Genet. 19 (2010) 3266–3281, https://doi.org/10.1093/hmg/ddq235.

[12] C. Bertoni, S. Jarrahian, T.M. Wheeler, Y. Li, E.C. Olivares, M.P. Calos, T.A. Rando, Enhancement of plasmid-mediated gene therapy for muscular dystrophy by directed plasmid integration, Proc. Natl. Acad. Sci. U. S. A. 103 (2006) 419–424, https://doi.org/10.1073/pnas.0504505102.

[13] C. Bertoni, Emerging gene editing strategies for Duchenne muscular dystrophy targeting stem cells, Front. Physiol. 5 (2014) 148, https://doi.org/10.3389/fphys.2014.00148.

[14] E. Berardi, D. Annibali, M. Cassano, S. Crippa, M. Sampaolesi, Molecular and cell-based therapies for muscle degenerations: a road under construction, Front. Physiol. 5 (2014) 119, https://doi.org/10.3389/fphys.2014.00119.

[15] N.A. Dumont, Y.X. Wang, J. von Maltzahn, A. Pasut, C.F. Bentzinger, C.E. Brun, M. A. Rudnicki, Dystrophin expression in muscle stem cells regulates their polarity and asymmetric division, Nat. Med. 21 (2015) 1455–1463, https://doi.org/10.1038/nm.3990.

[16] V. Mouly, A. Aamiri, A. Bigot, R.N. Cooper, S. Di Donna, D. Furling, T. Gidaro, V. Jacquemin, K. Mamchaoui, E. Negroni, S. Périé, V. Renault, S.D. Silva-Barbosa, G.S. Butler-Browne, The mitotic clock in skeletal muscle regeneration, disease and cell mediated gene therapy, Acta Physiol. Scand. 184 (2005) 3–15, https://doi.org/10.1111/j.1365-201X.2005.01417.x.

[17] A. Sacco, F. Mourkioti, R. Tran, J. Choi, M. Llewellyn, P. Kraft, M. Shkreli, S. Delp, J.H. Pomerantz, S.E. Artandi, H.M. Blau, Short telomeres and stem cell exhaustion model Duchenne muscular dystrophy in mdx/mTR mice, Cell 143 (2010) 1059–1071, https://doi.org/10.1016/j.cell.2010.11.039.

[18] C. Jiang, Y. Wen, K. Kuroda, K. Hannon, M.A. Rudnicki, S. Kuang, Notch signaling deficiency underlies age-dependent depletion of satellite cells in muscular dystrophy, Dis. Model. Mech. 7 (2014) 997–1004, https://doi.org/10.1242/dmm.015917.

[19] L. Rodriguez-Outeiriño, F. Hernandez-Torres, F.R. de Acuña, A. Rastrojo, C. Creus, A. Carvajal, L. Salmeron, M. Montolio, P. Soblechero-Martin, V. Arechavala-Gomeza, D. Franco, A.E. Aranega, miR-106b is a novel target to promote muscle regeneration and restore satellite stem cell function in injured Duchenne dystrophic muscle, Mol. Ther. - Nucleic Acids 29 (2022) 769–786, https://doi.org/10.1016/j.omtn.2022.08.025.

[20] I. Desguerre, M. Mayer, F. Leturcq, J.-P. Barbet, R.K. Gherardi, C. Christov, Endomysial fibrosis in Duchenne muscular dystrophy: a marker of poor outcome associated with macrophage alternative activation, J. Neuropathol. Exp. Neurol. 68 (2009) 762–773, https://doi.org/10.1097/NEN.0b013e3181aa31c2.

[21] S. Kim, K.A. Campbell, D.J. Fox, D.J. Matthews, R. Valdez, Corticosteroid Treatments in Males With Duchenne Muscular Dystrophy: Treatment Duration and Time to Loss of Ambulation, J. Child Neurol. 30 (2015) 1275–1280, https://doi.org/10.1177/0883073814558120.

[22] S. Kourakis, C.A. Timpani, D.G. Campelj, P. Hafner, N. Gueven, D. Fischer, E. Rybalka, Standard of care versus new-wave corticosteroids in the treatment of Duchenne muscular dystrophy: Can we do better? Orphanet J. Rare Dis. 16 (2021), 117 https://doi.org/10.1186/s13023-021-01758-9.

[23] Z. Ma, Z. Zhong, Z. Zheng, X.-M. Shi, W. Zhang, Inhibition of glycogen synthase kinase-3β attenuates glucocorticoid-induced suppression of myogenic differentiation in vitro, PloS One 9 (2014), e105528, https://doi.org/10.1371/journal.pone.0105528.

[24] O. Schakman, H. Gilson, J.P. Thissen, Mechanisms of glucocorticoid-induced myopathy, J. Endocrinol. 197 (2008) 1–10, https://doi.org/10.1677/JOE-07-0606.

[25] L. Wang, J. Li, L.-J. Di, Glycogen synthesis and beyond, a comprehensive review of GSK3 as a key regulator of metabolic pathways and a therapeutic target for treating metabolic diseases, Med. Res. Rev. 42 (2022) 946–982, https://doi.org/10.1002/med.21867.

[26] J. von Maltzahn, N.C. Chang, C.F. Bentzinger, M.A. Rudnicki, Wnt signaling in myogenesis, Trends Cell Biol. 22 (2012) 602–609, https://doi.org/10.1016/j.tcb.2012.07.008.

[27] S. Tajbakhsh, U. Borello, E. Vivarelli, R. Kelly, J. Papkoff, D. Duprez, M. Buckingham, G. Cossu, Differential activation of Myf5 and MyoD by different Wnts in explants of mouse paraxial mesoderm and the later activation of myogenesis in the absence of Myf5, Dev. Camb. Engl. 125 (1998) 4155–4162, https://doi.org/10.1242/dev.125.21.4155.

[28] A.E. Münsterberg, J. Kitajewski, D.A. Bumcrot, A.P. McMahon, A.B. Lassar, Combinatorial signaling by Sonic hedgehog and Wnt family members induces myogenic bHLH gene expression in the somite, Genes Dev. 9 (1995) 2911–2922, https://doi.org/10.1101/gad.9.23.2911.

[29] A.S. Brack, I.M. Conboy, M.J. Conboy, J. Shen, T.A. Rando, A temporal switch from notch to Wnt signaling in muscle stem cells is necessary for normal adult myogenesis, Cell Stem Cell 2 (2008) 50–59, https://doi.org/10.1016/j.stem.2007.10.006.

[30] N. Kurgan, K.C. Whitley, L.A. Maddalena, F. Moradi, J. Stoikos, S.I. Hamstra, E. A. Rubie, M. Kumar, B.D. Roy, J.R. Woodgett, J.A. Stuart, V.A. Fajardo, A Low-Therapeutic Dose of Lithium Inhibits GSK3 and Enhances Myoblast Fusion in C2C12 Cells, Cells 8 (2019) 1340, https://doi.org/10.3390/cells8111340.

[31] M. Martin, K. Rehani, R.S. Jope, S.M. Michalek, Toll-like receptor—mediated cytokine production is differentially regulated by glycogen synthase kinase 3, Nat. Immunol. 6 (2005) 777–784, https://doi.org/10.1038/ni1221.

[32] H. Wang, J. Brown, Z. Gu, C.A. Garcia, R. Liang, P. Alard, E. Beurel, R.S. Jope, T. Greenway, M. Martin, Convergence of the Mammalian Target of Rapamycin Complex 1- and Glycogen Synthase Kinase 3-β–Signaling Pathways Regulates the Innate Inflammatory Response, J. Immunol. Baltim. Md 1950 186 (2011) 5217–5226, https://doi.org/10.4049/jimmunol.1002513.

[33] N. de Pedro, J. Cantizani, F.J. Ortiz-López, V. González-Menéndez, B. Cautain, L. Rodríguez, G.F. Bills, F. Reyes, O. Genilloud, F. Vicente, Protective effects of isolecanoric acid on neurodegenerative in vitro models, Neuropharmacology 101 (2016) 538–548, https://doi.org/10.1016/j.neuropharm.2015.09.029.

[34] A. Sakurai, Y. Goto, Chemical Studies on the Lichen. I. The Structure of Isolecanoric Acid, a New ortho-Depside Isolated from Parmelia tinctorum Despr, Bull. Chem. Soc. Jpn. 60 (1987) 1917–1918, https://doi.org/10.1246/bcsj.60.1917.

[35] G. Toda, T. Yamauchi, T. Kadowaki, K. Ueki, Preparation and culture of bone marrow-derived macrophages from mice for functional analysis, STAR Protoc. 2 (2020), 100246, https://doi.org/10.1016/j.xpro.2020.100246.

[36] W. Ying, P.S. Cheruku, F.W. Bazer, S.H. Safe, B. Zhou, Investigation of Macrophage Polarization Using Bone Marrow Derived Macrophages, J. Vis. Exp. JoVE (2013) 50323, https://doi.org/10.3791/50323.

[37] F. Annang, G. Pérez-Moreno, C. Díaz, V. González-Menéndez, N. de Pedro Montejo, J.P. Del Palacio, P. Sánchez, S. Tanghe, A. Rodriguez, I. Pérez-Victoria, J. Cantizani, L.M. Ruiz-Pérez, O. Genilloud, F. Reyes, F. Vicente, D. González-Pacanowska, Preclinical evaluation of strasseriolides A-D, potent antiplasmodial macrolides isolated from Strasseria geniculata CF-247,251, Malar. J. 20 (2021), 457, https://doi.org/10.1186/s12936-021-03993-8.

[38] V. Corpas-López, M. Díaz-Gavilán, F. Franco-Montalbán, G. Merino-Espinosa, M. López-Viota, J. López-Viota, E. Belmonte-Reche, J. Pérez-Del Palacio, N. de Pedro, J.A. Gómez-Vidal, F. Morillas-Márquez, J. Martín-Sánchez, A nanodelivered Vorinostat derivative is a promising oral compound for the treatment of visceral leishmaniasis, Pharmacol. Res. 139 (2019) 375–383, https://doi.org/10.1016/j.phrs.2018.11.039.

[39] M. Finley, J. Cassaday, T. Kreamer, X. Li, K. Solly, G. O'Donnell, M. Clements, A. Converso, S. Cook, C. Daley, R. Kraus, M.-T. Lai, M. Layton, W. Lemaire, D. Staas, J. Wang, Kinetic Analysis of Membrane Potential Dye Response to NaV1.7 Channel Activation Identifies Antagonists with Pharmacological Selectivity against NaV1.5, J. Biomol. Screen. 21 (2016) 480–489, https://doi.org/10.1177/1087057116629669.

[40] R.M.J. Deacon, Measuring the strength of mice, J. Vis. Exp. JoVE (2013) 2610, https://doi.org/10.3791/2610.

[41] R. Benchaouir, M. Meregalli, A. Farini, G. D'Antona, M. Belicchi, A. Goyenvalle, M. Battistelli, N. Bresolin, R. Bottinelli, L. Garcia, Y. Torrente, Restoration of human dystrophin following transplantation of exon-skipping-engineered DMD patient stem cells into dystrophic mice, Cell Stem Cell 1 (2007) 646–657, https://doi.org/10.1016/j.stem.2007.09.016.

[42] D. Vallejo, F. Hernández-Torres, E. Lozano-Velasco, L. Rodriguez-Outeiriño, A. Carvajal, C. Creus, D. Franco, A.E. Aránega, PITX2 Enhances the Regenerative Potential of Dystrophic Skeletal Muscle Stem Cells, Stem Cell Rep. 10 (2018) 1398–1411, https://doi.org/10.1016/j.stemcr.2018.03.009.
[43] S. Cui, L. Li, R.T. Yu, M. Downes, R.M. Evans, J.-A. Hulin, H.P. Makarenkova, R. Meech, β-Catenin is essential for differentiation of primary myoblasts via cooperation with MyoD and α-catenin, Dev. Camb. Engl. 146 (2019) dev167080, https://doi.org/10.1242/dev.167080.
[44] A. Rudolf, E. Schirwis, L. Giordani, A. Parisi, C. Lepper, M.M. Taketo, F. Le Grand, β-Catenin Activation in Muscle Progenitor Cells Regulates Tissue Repair, Cell Rep. 15 (2016) 1277–1290, https://doi.org/10.1016/j.celrep.2016.04.022.
[45] E. Lozano-Velasco, D. Vallejo, F.J. Esteban, C. Doherty, F. Hernández-Torres, D. Franco, A.E. Aránega, A Pitx2-MicroRNA Pathway Modulates Cell Proliferation in Myoblasts and Skeletal-Muscle Satellite Cells and Promotes Their Commitment to a Myogenic Cell Fate, Mol. Cell. Biol. 35 (2015) 2892–2909, https://doi.org/10.1128/MCB.00536-15.
[46] W.G. Aschenbach, R.C. Ho, K. Sakamoto, N. Fujii, Y. Li, Y.-B. Kim, M.F. Hirshman, L.J. Goodyear, Regulation of dishevelled and beta-catenin in rat skeletal muscle: an alternative exercise-induced GSK-3beta signaling pathway, Am. J. Physiol. Endocrinol. Metab. 291 (2006) E152–E158, https://doi.org/10.1152/ajpendo.00180.2005.
[47] A. Reggio, M. Rosina, A. Palma, A. Cerquone Perpetuini, L.L. Petrilli, C. Gargioli, C. Fuoco, E. Micarelli, G. Giuliani, M. Cerretani, A. Bresciani, F. Sacco, L. Castagnoli, G. Cesareni, Adipogenesis of skeletal muscle fibro/adipogenic progenitors is affected by the WNT5a/GSK3/β-catenin axis, Cell Death Differ. 27 (2020) 2921–2941, https://doi.org/10.1038/s41418-020-0551-y.
[48] J.W. McGreevy, C.H. Hakim, M.A. McIntosh, D. Duan, Animal models of Duchenne muscular dystrophy: from basic mechanisms to gene therapy, Dis. Model. Mech. 8 (2015) 195–213, https://doi.org/10.1242/dmm.018424.
[49] R. Kettenhofen, H. Bohlen, Preclinical assessment of cardiac toxicity, Drug Discov. Today 13 (2008) 702–707, https://doi.org/10.1016/j.drudis.2008.06.011.
[50] B.N. Ames, J. Mccann, E. Yamasaki, Methods for detecting carcinogens and mutagens with the Salmonella/mammalian-microsome mutagenicity test, Mutat. Res. 31 (1975) 347–364, https://doi.org/10.1016/0165-1161(75)90046-1.
[51] D. Duan, N. Goemans, S. Takeda, E. Mercuri, A. Aartsma-Rus, Duchenne muscular dystrophy, Nat. Rev. Dis. Prim. 7 (2021), 13, https://doi.org/10.1038/s41572-021-00248-3.
[52] R. Cortés-Vieyra, O. Silva-García, A. Gómez-García, S. Gutiérrez-Castellanos, C. Álvarez-Aguilar, V.M. Baizabal-Aguirre, Glycogen Synthase Kinase 3β Modulates the Inflammatory Response Activated by Bacteria, Viruses, and Parasites, Front. Immunol. 12 (2021), 675751, https://doi.org/10.3389/fimmu.2021.675751.
[53] Y. Zheng, P.-P. Ye, Y. Zhou, S.-Y. Wu, X.-T. Liu, B. Du, B.-H. Tang, M. Kan, A.-Q. Nie, R. Yin, M. Wang, G.-X. Hao, L.-L. Song, X.-M. Yang, X. Huang, L.-Q. Su, W.-Q. Wang, J. van den Anker, W. Zhao, LPS-Induced Inflammation Affects Midazolam Clearance in Juvenile Mice in an Age-Dependent Manner, J. Inflamm. Res. 14 (2021) 3697–3706, https://doi.org/10.2147/JIR.S321492.
[54] M. Theret, M. Saclier, G. Messina, F.M.V. Rossi, Macrophages in skeletal muscle dystrophies, an entangled partner, J. Neuromuscul. Dis. 9 (2022) 1–23, https://doi.org/10.3233/JND-210737.
[55] A.S. Rosenberg, M. Puig, K. Nagaraju, E.P. Hoffman, S.A. Villalta, V.A. Rao, L. M. Wakefield, J. Woodcock, Immune-mediated pathology in Duchenne muscular dystrophy, Sci. Transl. Med. 7 (2015) 299rv4, https://doi.org/10.1126/scitranslmed.aaa7322.
[56] H.M. Blau, C. Webster, G.K. Pavlath, Defective myoblasts identified in Duchenne muscular dystrophy, Proc. Natl. Acad. Sci. U. S. A. 80 (1983) 4856–4860, https://doi.org/10.1073/pnas.80.15.4856.
[57] J.V. Pham, M.A. Yilma, A. Feliz, M.T. Majid, N. Maffetone, J.R. Walker, E. Kim, H. J. Cho, J.M. Reynolds, M.C. Song, S.R. Park, Y.J. Yoon, A Review of the Microbial Production of Bioactive Natural Products and Biologics, Front. Microbiol. 10 (2019), 1404, https://doi.org/10.3389/fmicb.2019.01404.
[58] D.J. Newman, G.M. Cragg, Natural Products as Sources of New Drugs over the Nearly Four Decades from 01/1981 to 09/2019, J. Nat. Prod. 83 (2020) 770–803, https://doi.org/10.1021/acs.jnatprod.9b01285.
[59] H. Yin, F. Price, M.A. Rudnicki, Satellite Cells and the Muscle Stem Cell Niche, Physiol. Rev. 93 (2013) 23–67, https://doi.org/10.1152/physrev.00043.2011.
[60] A.E. Aránega, E. Lozano-Velasco, L. Rodriguez-Outeiriño, F. Ramírez de Acuña, D. Franco, F. Hernández-Torres, MiRNAs and Muscle Regeneration: Therapeutic Targets in Duchenne Muscular Dystrophy, Int. J. Mol. Sci. 22 (2021) 4236, https://doi.org/10.3390/ijms22084236.
[61] P. Cisternas, C.P. Vio, N.C. Inestrosa, Role of Wnt signaling in tissue fibrosis, lessons from skeletal muscle and kidney, Curr. Mol. Med. 14 (2014) 510–522, https://doi.org/10.2174/1566524014666140414210346.
[62] K.C. Whitley, S.I. Hamstra, R.W. Baranowski, C.J.F. Watson, R.E.K. MacPherson, A. J. MacNeil, B.D. Roy, R. Vandenboom, V.A. Fajardo, GSK3 inhibition with low dose lithium supplementation augments murine muscle fatigue resistance and specific force production, Physiol. Rep. 8 (2020), e14517, https://doi.org/10.14814/phy2.14517.
[63] W.F. Theeuwes, H.R. Gosker, R.C.J. Langen, K.J.P. Verhees, N. a M. Pansters, A.M. W.J. Schols, A.H.V. Remels, Inactivation of glycogen synthase kinase-3β (GSK-3β) enhances skeletal muscle oxidative metabolism, Biochim. Biophys. Acta Mol. Basis Dis. 1863 (2017) 3075–3086, https://doi.org/10.1016/j.bbadis.2017.09.018.
[64] N.A.M. Pansters, A.M.W.J. Schols, K.J.P. Verhees, C.C. de Theije, F.J. Snepvangers, M.C.J.M. Kelders, N.D.J. Ubags, A. Haegens, R.C.J. Langen, Muscle-specific GSK-3β ablation accelerates regeneration of disuse-atrophied skeletal muscle, Biochim. Biophys. Acta 1852 (2015) 490–506, https://doi.org/10.1016/j.bbadis.2014.12.006.
[65] Y.X. Wang, P. Feige, C.E. Brun, B. Hekmatnejad, N.A. Dumont, J.-M. Renaud, S. Faulkes, D.E. Guindon, M.A. Rudnicki, EGFR-Aurka Signaling Rescues Polarity and Regeneration Defects in Dystrophin-Deficient Muscle Stem Cells by Increasing Asymmetric Divisions, Cell Stem Cell 24 (2019) 419–432.e6, https://doi.org/10.1016/j.stem.2019.01.002.
[66] E. Villa-Moruzzi, F. Puntoni, O. Marin, Activation of protein phosphatase-1 isoforms and glycogen synthase kinase-3 beta in muscle from mdx mice, Int. J. Biochem. Cell Biol. 28 (1996) 13–22, https://doi.org/10.1016/1357-2725(95)00119-0.
[67] S. Junyent, J.C. Reeves, J.L. Szczerkowski, C.L. Garcin, T.-J. Trieu, M. Wilson, J. Lundie-Brown, S.J. Habib, Wnt- and glutamate-receptors orchestrate stem cell dynamics and asymmetric cell division, eLife 10 (2021), e59791, https://doi.org/10.7554/eLife.59791.
[68] B. De Paepe, J.L. De Bleecker, Cytokines and Chemokines as Regulators of Skeletal Muscle Inflammation: Presenting the Case of Duchenne Muscular Dystrophy, Mediat. Inflamm. 2013 (2013), e540370, https://doi.org/10.1155/2013/540370.
[69] V. Malik, L.R. Rodino-Klapac, J.R. Mendell, Emerging drugs for Duchenne muscular dystrophy, Expert Opin. Emerg. Drugs 17 (2012) 261–277, https://doi.org/10.1517/14728214.2012.691965.
[70] J. Dort, Z. Orfi, P. Fabre, T. Molina, T.C. Conte, K. Greffard, O. Pellerito, J.-F. Bilodeau, N.A. Dumont, Resolvin-D2 targets myogenic cells and improves muscle regeneration in Duchenne muscular dystrophy, Nat. Commun. 12 (2021), 6264, https://doi.org/10.1038/s41467-021-26516-0.